Impacts of Air-sea Interactions on Regional Air Quality Predictions Using a Coupled Atmosphere-ocean Model in Southeastern U.S.

Jian He, Ruoying He, Yang Zhang[*]

Department of Marine, Earth, and Atmospheric Sciences, North Carolina State University, Raleigh, NC 27695, USA

ABSTRACT

Air-sea interactions have significant impacts on coastal convection and surface fluxes exchange. They are important for the spatial and vertical distributions of air pollutants that affect public health, particularly in densely populated coastal areas. To understand the impacts of air-sea interactions on coastal air quality predictions, sensitivity simulations with different atmosphere-ocean coupling are conducted in this work over southeastern U.S. in July 2010 using the Weather Research and Forecasting Model with Chemistry (WRF/Chem). The results show that comparing to WRF/Chem without air-sea interactions, WRF/Chem with a 1-D ocean mixed layer model (WRF/Chem-OML) and WRF/Chem coupled with a 3-D Regional Ocean Modeling System (WRF/Chem-ROMS) predict the domain averaged changes in the sea surface temperature of 0.06°C and 0.94°C, respectively for July average. The simulated differences in the surface concentrations of O_3 and $PM_{2.5}$ between WRF/Chem-ROMS and WRF/Chem can be as large as 17.3 ppb and 7.9 µg m^{-3}, respectively, with the largest changes occurring not only along coast and remote ocean, but also over some inland areas. Extensive validations against observations show that WRF/Chem-ROMS improves the predictions of most cloud and radiative variables, and surface concentrations of some chemical species such as SO_2, NO_2, maximum 1-h and 8-h O_3, SO_4^{2-}, NH_4^+, NO_3^-, and PM_{10}. This illustrates the benefits and needs of using coupled atmosphere-ocean model with advanced model representations of air-sea interactions for regional air quality modeling.

Keywords: O_3; $PM_{2.5}$; Air-sea interaction; WRF/Chem; ROMS; COAWST; Coupled atmosphere-ocean model.

INTRODUCTION

3-D regional atmospheric models are often used for regional air quality studies at spatial resolutions of 4–36 km. Examples of such models include the Weather Research and Forecasting model with chemistry (WRF/Chem, Grell *et al.*, 2005; Fast *et al.*, 2006; Zhang *et al.*, 2010), the Community Multi-scale Air Quality (CMAQ, Binkowski and Roselle, 2003; Byun and Schere, 2006) model, and the Comprehensive Air Quality Model with Extensions (CAMx, ENVIRON, 1998, 2010). Most regional models consist of an atmospheric component coupled to a land surface scheme and forced by prescribed sea surface temperature (SST) over ocean (Chen *et al.*, 2011; Seo *et al.*, 2014). However, there is a complicate relationship between SST perturbation and the subsequent heating in the atmosphere (Kushnir and Held, 1996). For example, SST perturbation can impact atmospheric circulation and variability (Brayshaw *et al.*, 2011; Keeley *et al.*, 2012). As a result, boundary layer

conditions are impacted through air-sea interactions, resulting in changes in the planetary boundary layer height (PBLH), surface temperature, and surface wind. Most coastal areas contain dense population. The air pollutants such as ozone (O_3) and particulate matter (PM) trapped in the boundary layer of these regions can have adverse impacts on human health and environment. The changes in the horizontal SST gradients can impact the surface fluxes at atmosphere-ocean interface, which leads to the changes in convection and PBLH. Both have significant impacts on the temporal and spatial distributions of dust, sea-salt emissions and chemical species that in turn affect human health, environment, and ecology. As such, it is also important to include the representations of air-sea interactions in regional air quality studies.

Modeling air-sea interaction process is an active field of research in oceanography. For example, Warner *et al.* (2010) reported the Coupled Ocean-Atmosphere-Wave-Sediment Transport (COAWST) Modeling System, which couples the atmosphere model WRF (Skamarock *et al.*, 2008), with the Regional Ocean Modeling System (ROMS, Shchepetkin *et al.*, 2005) (hereafter WRF-ROMS). The coupling system has been applied for a number of regional air-sea interaction studies (Nelson and He, 2012; Nelson *et al.*, 2014; Zambon *et al.*, 2014a, b), with a focus on the effects of air-sea

---
[*]Corresponding author.
 Tel.: 1-919-515-9688; Fax: 1-919-515-7802
 E-mail address: yang_zhang@ncsu.edu

interactions on atmospheric dynamics and ocean circulation. While many of these coupled modeling systems (i.e., only coupling physical atmosphere with ocean) include prescribed or constant chemistry (e.g., prescribed O_3 or AOD), little work has been done using coupled regional air quality and regional ocean model (i.e., coupling both physical and chemical atmosphere with ocean). Meteorology is important for distribution and concentration of air pollutants (e.g., transport of air pollutants, photolysis, and chemical reactions). On the other hand, chemical species can influence the meteorological and cloud/radiative variables by perturbing the atmospheric radiation budget and through cloud properties. In this work, building on existing coupled WRF-ROMS within the framework of COAWST version 3.1, WRF/Chem version 3.6.1 is coupled with ROMS version 3.7 (hereafter WRF/Chem-ROMS) in COAWST to study the effects of air-sea interactions on regional air quality. The main objective in this work is to examine the impacts of air-sea interactions on model predictions of meteorology, chemistry, and cloud/radiation over coastal regions.

MODEL CONFIGURATIONS AND EVALUATION PROTOCOLS

Model Description and Setup

The WRF/Chem model (Grell *et al.*, 2005; Fast *et al.*, 2006) is used in this work to represent the atmospheric conditions. It is based on WRF/Chem version 3.6.1 with additional modifications and updates by Wang *et al.* (2015a). The major updates include (1) the coupling of the 2005 Carbon Bond (CB05) gas-phase (Yarwood *et al.*, 2005; Sarwar *et al.*, 2008) with the existing Modal of Aerosol Dynamics in Europe with the Volatility Basis Set approach for simulating secondary organic aerosol (SOA) (MADE-VBS, Grell *et al.*, 2005; Ahmadov *et al.*, 2012); (2) incorporating the aqueous chemistry (AQChem) module of CMAQ version 5.0 (Sarwar *et al.*, 2011) into WRF/Chem. This new chemistry-aerosol option of CB05-MADE/VBS has been coupled with existing model treatments and demonstrated its capability to simulate chemistry-aerosol-radiation-cloud feedbacks such as aerosol semi-direct effects on photolysis rates of major gases, aerosol indirect effects

on cloud droplet numbers, and cloud effects on shortwave radiation (Yahya *et al.*, 2014; Wang *et al.*, 2015a, b; Yahya *et al.*, 2015). In this work, this chemistry-aerosol option of CB05-MADE/VBS is applied for all the WRF/Chem simulations.

Table 1 shows the simulations conducted in this work. The WRF/Chem simulations are conducted over southeastern U.S. for July 2010, with a 12-km horizontal resolution (i.e., 160×210 grid cells) and a vertical resolution of 35 layers from the surface to 100 hPa, with a surface layer model height of 38 m. The emissions for WRF/Chem are from Wang *et al.* (2015b), which is based on the 2008 National Emission Inventory (NEI) (version 2, released April 10, 2012). The meteorological initial and boundary conditions (ICs and BCs) are generated from the National Center for Environmental Prediction Final Analysis (NCEP-FNL) and the chemical ICs and BCs are from the Community Earth System Model (CESM) every 6-hour output (He *et al.*, 2015). The physics options used for all the simulations in this work are summarized in Table 1 of Wang *et al.* (2015a), except for the cumulus parameterization scheme. In Wang *et al.* (2015a) (refer to as W15 hereafter), the cumulus parameterization scheme was based on Grell 3D ensemble scheme (referred to as G3D, Grell and Devenyi, 2002; Grell and Freitas, 2014), which allows for a series of different assumptions that are commonly used in convective parameterizations and includes options to spread subsidence to neighboring grid points. This work uses the cumulus parameterization scheme of Grell and Freitas (2014) (referred to as GF scheme), which allows for subgrid scale convection representation. The choice of GF scheme is based on the comprehensive comparison of model results between simulations with G3D scheme (i.e., W15) and GF scheme (i.e., SEN1) (see Table 1). The rational of such a choice and relevant performance evaluation can be found in the supplementary material (see Tables S1(a)–1(b), and Figs. S1(a)–1(b) and S2(a)–2(b)). In addition to the options listed in Table 1 of W15, SEN1 includes prescribed SST forcing from NCEP by updating every 6-hour.

SEN2 is configured same as SEN1 but with the 1-dimensional (1-D) ocean mixed layer (OML) model of Pollard *et al.* (1973) turned on (hereafter WRF/Chem-OML).

Table 1. Simulation Design.

Run Index	Description	Purpose
W15	Based on Wang *et al.* (2015a), NCSU's version of WRF/Chem v3.6.1 with the G3 cumulus parameterization	Served as baseline
SEN1	Same as W15, but with the GF cumulus parameterization	The differences between SEN1 and W15 indicate the impacts of different cumulus parameterizations on model predictions; Served as the baseline to investigate the impacts of atmosphere-ocean coupling using 1-D OML and 3-D ROMS.
SEN2	Same as SEN1, but with WRF/Chem with the 1-D ocean mixed layer model (WRF/Chem-OML)	The differences between SEN2 and SEN1 indicate the impacts of 1-D ocean mixed layer model on model predictions
SEN3	Same as SEN1, but with WRF/Chem coupled with ROMS within the COAWST frame work (WRF/Chem-ROMS)	The differences between SEN3 and SEN1 indicate the impacts of the atmosphere-ocean coupling on model predictions

The 1-D OML model includes the wind-driven ocean mixing and mixed layer deepening process. The surface wind stress generates currents in the ocean mixed layer (typically 30–100 m deep), which leads to mixing with cooler water below. The model does not consider the pressure gradients or horizontal advection, but does include the Coriolis effect, which is important for the rotation of inertial currents and SST cooling. The 1-D OML model represents a simple balance between the local rate of change of ocean temperature and the net surface heat flux. Negative (positive) net heat flux leads to a cooling (warming) trend of ocean temperature, which in turn affects marine boundary layer stability, air temperature, and surface wind distributions (e.g., Chelton *et al.*, 2007). The initial mixed layer depth (i.e., 50 m) and temperature lapse rate (i.e., 0.14 K m^{-1}) are specified in the model for the entire domain, which is a main source of uncertainty considering spatial variations. The OML model is called every model time step (i.e., 60 seconds) across every grid point and the SST is then fed back into the atmospheric model (i.e., WRF/Chem).

SEN3 has the same WRF/Chem configuration as SEN1, but with fully coupling with ROMS (updated through August 2014) (i.e., WRF/Chem-ROMS). ROMS is a 3-dimentional (3-D), free-surface, hydrostatic, and primitive equations ocean model, which uses vertically stretched terrain-following (σ) coordinates combined with advanced physics packages to allow simulation of advective processes, Coriolis, and viscosity in 3-dimensions. It includes the high-order advection and time-stepping schemes, weighted temporal averaging of the barotropic mode, conservative parabolic splines for vertical discretization, and the barotropic pressure gradient term, which can be applied for estuarine, coastal and basin-scale oceanic processes (Marchesiello *et al.*, 2003; He and Wilkin, 2006; He *et al.*, 2008). The COAWST (Warner *et al.*, 2010) modeling system is designed to enable the integration of oceanic, atmospheric, wave, and morphological processes in the coastal ocean. It consists of three state-of-the-art numerical models representing the atmosphere (i.e., WRF), ocean (i.e., ROMS) and wave (i.e., Simulating WAves Nearshore, SWAN) conditions as well as the sediment transport representation using the Model Coupling Toolkit (MCT). COAWST represents the frontier in regional air-sea interaction modeling. There are different options to configure the model with the coupling of WRF and ROMS only, the coupling of WRF, ROMS, and SWAN, or with all components turned on. In this work, only the WRF and ROMS coupling is turned on. The coupling of WRF/Chem-ROMS (i.e., SEN3) is within the framework of COAWST, via MCT as the coupler.

The original COAWST system is configured for a two-way coupling only between WRF and ROMS. In this work, NCSU's version of WRF/Chem replaces WRF and is coupled with ROMS within the COAWST system to provide insights about the effects of air-sea interactions on coastal air quality. ROMS is configured on the same grid resolution as WRF/Chem with 157 interior density (ρ) points in the Y direction and 207 interior ρ points in the X direction, and with 16 layers vertically in the ocean. The initial and boundary conditions are from the global HYbrid Coordinate

Ocean Model (HYCOM) combined with the Navy Coupled Ocean Data Assimilation (NCODA) (http://tds.hycom.org/ thredds/catalog.html). HYCOM is a high resolution global analysis dataset (1/12°) with data frequency on a daily basis. This resolution is very close to the grid resolution of 12-km used in this work. For other datasets, they either have relatively coarse grid resolutions (e.g., the Simple Ocean Data Assimilation, SODA, http://www.atmos.umd. edu/~ocean/data.html) or their data frequency is on a monthly basis (e.g., the Global Ocean Physical Reanalysis System, GLORS, http://www.cmcc.it/it/models/c-glors-the-cmcc-global-ocean-physical-reanalysis-system), which can result in large biases when they are interpolated into the model grid resolution or time period. The coastline and bathymetry are extracted from the Global Self-consistent Hierarchical High-resolution Shorelines (GSHHS), and 5-Minute Gridded Global Relief Data Collection (ETOPO5), respectively. Fig. 1 shows a diagram of the coupling WRF/Chem with ROMS within the COAWST framework. ROMS is coupled with WRF through MCT. SST is computed inside ROMS and then passed to WRF/Chem. Meanwhile, several variables are passed from WRF/Chem to ROMS, including net heat flux and wind stress. The time step for ROMS calculation is 30 seconds and the time frequency for the WRF/Chem-ROMS coupling is 10 minutes. This study focuses on the synoptic, meso-scale dynamics of both ocean and atmosphere, which require the coupled modeling system to resolve air-sea flux exchange process as frequently as computationally possible. The choice of 10 mins provides a good balance between the model physics and computational demands associated with system coupling. The simulations are conducted for entire July 2010, with 7 days (June 24–30, 2014) for spinup. The model output frequency is hourly.

Unlike SEN1 that does not include any air-sea interactions, both SEN2 and SEN3 include air-sea interactions but with varying degrees of details. Fig. 2 shows the schematic diagram of major atmospheric processes treated in SEN1, SEN2, and SEN3 and major processes associated with air-sea interactions that affect coastal air quality treated in SEN2 and SEN3. As shown in Fig. 2, air-sea interactions affect marine boundary layers through exchange of heat and momentum fluxes, which would further affect large scale circulation, cloud formation, and precipitation. Over coastal areas, emissions over both inland areas (e.g., biogenic emissions and anthropogenic emissions) and oceanic areas (e.g., emissions from shipping and natural sources such as sea spray and phytoplankton) can generate secondary air pollutants through chemical transformation (e.g., photochemical oxidation, nighttime chemistry) and aerosol microphysics (e.g., gas-to-particle conversion) (note that emissions from phytoplankton are not included in this work). Air pollutants can further affect cloud properties through chemical reactions (e.g., heterogeneous and aqueous-phase chemical reactions) or microphysical processes (e.g., condensation/evaporation, aerosol activation, ice nucleation). They can be transported through large-scale circulation or long-range transport, and removed from atmosphere through dry and wet deposition. The coupling of air-sea interactions can provide more comprehensive representations
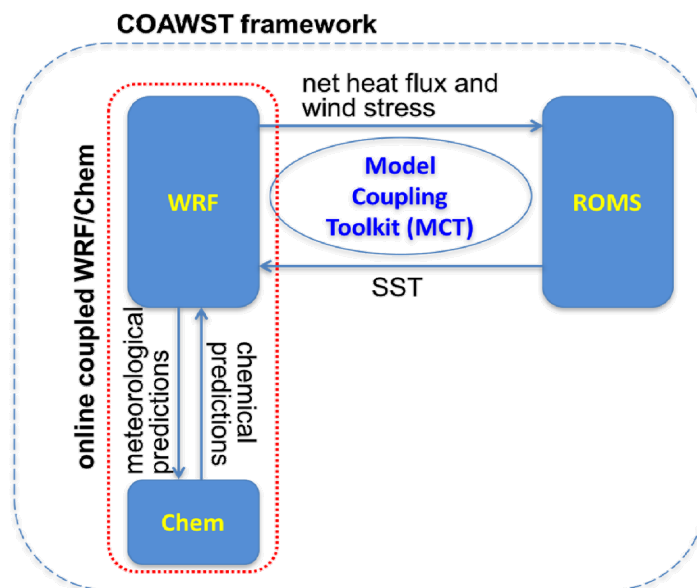
Fig. 1. Diagram of WRF/Chem-ROMS coupling within COAWST. The net heat flux and wind stress are passed from WRF to ROMS. The sea surface temperature (SST) is passed from ROMS to WRF. WRF passes predictions of meteorology to its chemistry package. Chemical predictions are passed from the chemistry package to WRF. The two-way coupling between WRF/Chem allows the simulation of feedbacks between chemistry/aerosol and meteorological variables. The two-way coupling between WRF and ROMS allows dynamic interactions between atmosphere and ocean.
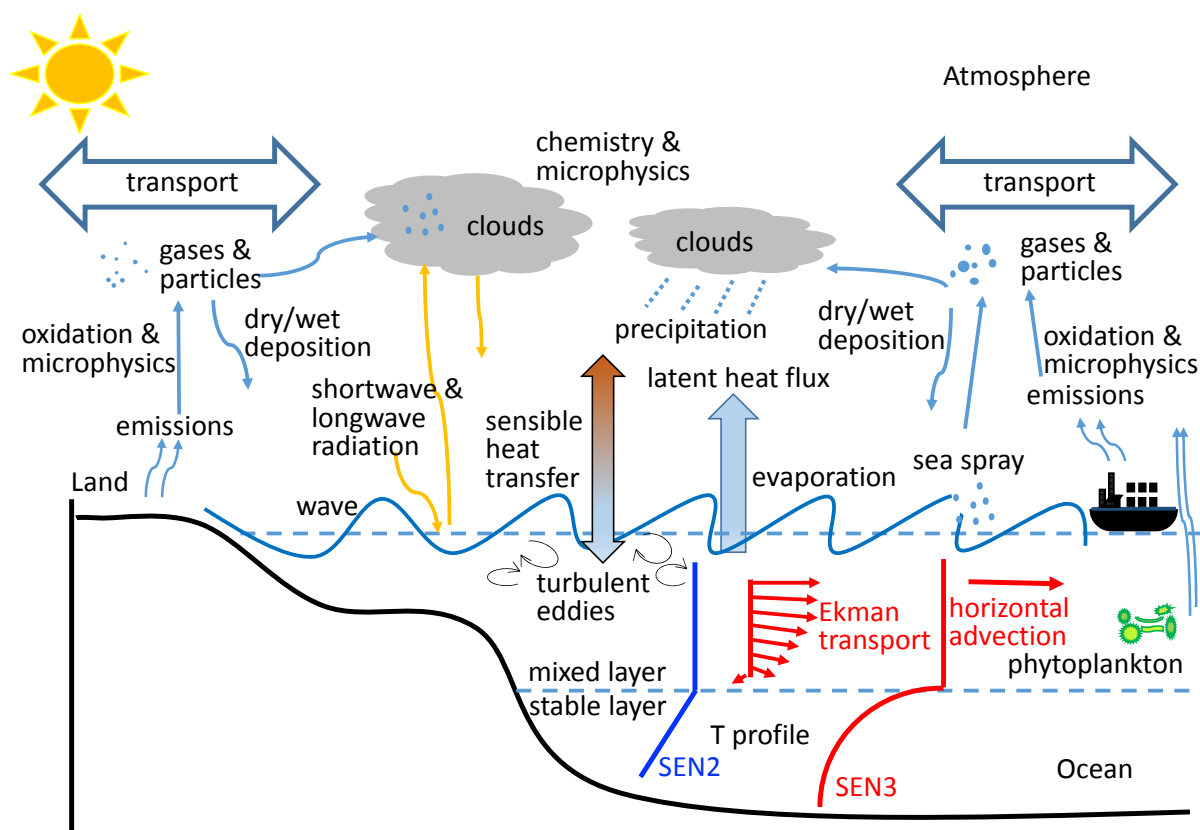

Fig. 2. The schematic diagram of processes associated with air-sea interactions that affect coastal air quality. In atmosphere, the yellow arrows represent the shortwave and longwave radiation. The blue arrows represent all other physical and chemical processes. In ocean, the temperature profile by SEN2 (i.e., 1-D ocean mixed layer model) (in blue) uses specified temperature lapse rate below mixed layer from observations or climatology. The temperature profile by SEN3 (i.e., the 3-D ROMS model) (in red) calculates temperature lapse rate below mixed layer in ROMS. SEN3 also includes horizontal advection and Ekman transport processes (in red), which are not included in SEN2.

of associated processes for coastal air quality study. Fig. 2 also shows the main difference between SEN2 and SEN3, which is the calculation for ocean temperatures below mixed layer. While SEN2 uses specified temperature lapse rate from observations or climatology, SEN3 calculates temperature lapse rate in ROMS. In addition, SEN3 includes horizontal advection and Ekman transport processes, which are not included in SEN2. Such differences between SEN2 and SEN 3 will affect simulations of SST gradients and the exchanges for heat fluxes and momentum fluxes between

atmosphere and ocean surface.

Available Measurements and Evaluation Protocols

A number of observational datasets from surface networks and satellites are used for model evaluation. They are summarized along with the variables to be evaluated in Table 2. Meteorological variables such as temperature at 2-m (T2), relative humidity at 2-m (RH2), wind speed at 10-m (WS10), and wind direction at 10-m (WD10) are evaluated against observations from the National Centers for

Table 2. Datasets for Model Evaluation.

Species/Variables	Dataset	Spatial (Temporal) Resolution
Temperature at 2-m (T2), Relative humidity at 2-m (RH2), Wind speed at 10-m (WS10)	Land: NCEI, SEARCH; Ocean: NDBC	400 sites (hourly), 7 sites (hourly); 15 sites (hourly)
Wind direction at 10-m (WD10)	NCEI	400 sites (hourly)
Planetary boundary layer height (PBLH)	NCEP/NARR	32-km (monthly)
Sea surface temperature (SST), sensible heat flux (SHFLX), latent heat flux (LHFLX)	OAFlux	1° (monthly)
Precipitation (Precip)	GPCP, TMAP	2.5° (monthly), 0.25° (daily)
Outgoing longwave radiation (OLR), Downwelling longwave radiation (LWD), Downwelling shortwave radiation (SWD), Shortwave cloud radiative forcing (SWCF), Longwave cloud radiative forcing (LWCF)	CERES-EBAF	1° (monthly)
Cloud fraction (CF), Cloud optical thickness (COT), Cloud liquid water path (LWP)	CERES-SYN1deg	1° (monthly)
Precipitating water vapor (PWV), Aerosol optical depth (AOD), Column cloud condensation nuclei (ocean) at S = 0.5% (CCN5),	MODIS	1° (monthly)
Cloud droplet number concentration (CDNC)	Bennartz (2007)	1° (monthly)
Max 1-h Ozone (O_3), Max 8-h O_3	CASTNET, AIRS-AQS	38 sites (hourly), 420 (hourly)
Hourly O_3	AIRS-AQS, SEARCH	420 (hourly), 7 sites (hourly)
Sulfur dioxide (SO_2), Nitric acid (HNO_3)	CASTNET	38 sites (weekly)
Carbon monoxide (CO), Nitrogen dioxide (NO_2)	SEARCH	7 sites (hourly)
Sulfate (SO_4^{2-}), Ammonium (NH_4^+), Nitrate (NO_3^-)	CASTNET, IMPROVE, STN	38 sites (weekly), 29 sites (3-day), 74 sites (3-day to weekly)
Organic carbon (OC)	IMPROVE, SEARCH	29 sites (3-day), 7 sites (daily)
Elementary carbon (EC), Total carbon (TC)	IMPROVE, STN, SEARCH	29 sites (3-day), 74 sites (3-day to weekly) 7 sites (daily)
Particulate matter with diameter less than and equal to 2.5 μm ($PM_{2.5}$)	IMPROVE, STN, SEARCH	29 sites (3-day), 74 sites (3-day to weekly), 7 sites (daily)
Particulate matter with diameter less than and equal to 10 μm (PM_{10})	AIRS-AQS	53 sites (hourly)
Tropospheric CO	MOPITT	1° (monthly)
Tropospheric SO_2, NO_2	SCIAMCHY	0.25° (monthly)
Tropospheric ozone residual (TOR)	OMI/MLS	1.25° (monthly)

NCEI: National Centers for Environmental Information; NDBC: National Data Buoy Center; NCEP/NAAR: National Centers for Environmental Prediction and North American Regional Reanalysis; OAFlux: Objectively Analyzed Air-Sea Fluxes; GPCP: the Global Precipitation Climatology Project; TMAP: Multi-satellite Precipitation Analysis from the Tropical Rainfall Measuring Mission; CERES-EBAF: Clouds and Earth's Radiant Energy System Energy Balanced And Filled data product; CERES-SYN1deg: CERES Synoptic product at 1° spatial resolution; MODIS: Moderate Resolution Imaging Spectroradiometer; OMI/MLS: the Aura Ozone Monitoring Instrument in combination with Aura Microwave Limb Sounder; MOPITT: the Measurements Of Pollution In The Troposphere; the Global Ozone Monitoring Experiment; SCIAMCHY: the SCanning Imaging Absorption spectroMeter for Atmospheric CHartographY; CASTNET: Clean Air Status and Trends Network; IMPROVE: Interagency Monitoring of Protected Visual Environments; STN: Speciation Trends Network; SEARCH: Southeastern Aerosol Research and Characterization; AIRS-AQS: the Aerometric Information Retrieval System-Air Quality System.

Table 2(a). Statistical Performance of Meteorological, Cloud, and Radiative Variables.

Species/Variables	Datasets	obs	SEN1				SEN2				SEN3			
			sim	NMB (%)	NME (%)	Corr	sim	NMB (%)	NME (%)	Corr	sim	NMB (%)	NME (%)	Corr
T2 (°C)	NCEI	26.6	25.4	–4.3	8.4	0.83	25.4	–4.3	8.4	0.83	25.4	–4.4	8.4	0.83
	NDBC	27.8	27.4	–1.4	3.4	0.89	27.4	–1.4	3.5	0.89	26.7	–3.7	6.0	0.74
	SEARCH	27.7	26.2	–5.3	8.4	0.78	26.3	–5.1	7.6	0.78	26.2	–5.4	7.8	0.78
RH2 (%)	NCEI	73.9	73.6	–0.4	14.3	0.69	73.6	–0.4	14.3	0.68	73.7	–0.2	14.3	0.69
	SEARCH	75.5	77.3	2.4	12.7	0.70	77.3	2.4	12.6	0.70	77.7	2.9	12.9	0.69
WS10 (m s⁻¹)[1]	NCEI	6.8	2.6	–61.3	63.6	0.20	2.6	–61.5	63.7	0.20	2.7	–60.6	63.1	0.21
	NDBC	5.5	6.1	10.6	34.4	0.47	6.1	10.1	34.5	0.47	5.9	7.1	30.6	0.56
	SEARCH	2.5	2.2	–12.6	34.4	0.17	2.2	–13.4	34.8	0.18	2.2	–14.2	34.3	0.20
Precip (mm day⁻¹)	GPCP (land)	4.1	5.4	31.7	46.1	0.36	5.4	31.9	44.9	0.38	5.3	29.5	40.6	0.35
	GPCP (ocean)	3.9	12.0	211.5	215.5	0.24	12.0	210.3	214.7	0.25	8.5	119.2	124.5	0.37
	TMPA (land)	3.8	5.4	42.2	58.8	0.27	5.4	42.4	57.6	0.28	5.3	39.8	53.2	0.23
	TMPA (ocean)	5.3	12.0	128.2	133.4	0.38	12.0	127.3	132.4	0.40	8.5	60.6	73.4	0.46
SWD (W m⁻²)[3]	CERES (land)	263.7	262.5	–0.5	8.5	0.40	261.6	–0.8	8.4	0.35	261.2	–0.9	7.7	0.35
	CERES (ocean)	266.1	211.4	–20.6	21.2	0.48	211.3	–20.6	21.3	0.48	229.6	–13.7	14.2	0.49
	CASTNET	272.4	299.7	10.0	34.6	0.88	298.8	9.7	35.1	0.88	299.3	9.9	34.3	0.88
	SEARCH	303.6	256.5	–15.5	41.5	0.78	257.2	–15.3	40.6	0.78	251.9	–17.0	41.5	0.79
OLR (W m⁻²)	CERES (land)	259.9	241.7	–7.0	7.2	0.64	240.8	–7.3	7.5	0.64	241.7	–7.0	7.1	0.61
	CERES (ocean)	253.7	201.1	–20.7	20.7	0.51	200.7	–20.9	20.9	0.51	211.1	–16.8	16.8	0.56
SWCF (W m⁻²)	CERES (land)	–45.9	–66.5	45.1	50.8	0.42	–66.5	45.1	50.9	0.42	–66.5	45.0	49.4	0.33
	CERES (ocean)	–56.6	–120.2	112.5	113.7	0.47	–119.4	111.2	112.4	0.47	–100.9	78.5	79.3	0.54
LWCF (W m⁻²)	CERES (land)	31.7	37.7	18.9	37.3	0.49	37.7	19.1	37.1	0.49	37.1	17.2	34.4	0.46
	CERES (ocean)	30.9	74.5	141.4	141.9	0.42	74.2	140.3	140.9	0.42	64.1	107.7	108.1	0.49
CF (%)	CERES (land)	46.3	45.8	–1.0	27.1	0.32	45.7	–1.2	27.4	0.32	45.9	–0.9	26.7	0.29
	CERES (ocean)	53.3	75.9	42.3	46.1	0.14	75.9	42.3	46.2	0.14	72.9	36.7	39.3	0.20
COT	CERES (land)	34.8	21.1	–39.5	53.0	–0.39	21.0	–39.8	52.2	–0.44	21.0	–39.8	49.9	–0.35
	CERES (ocean)	26.2	43.2	64.6	77.5	0.28	42.6	62.5	75.4	0.28	36.0	37.5	58.3	0.27
LWP (g m⁻²)	CERES (land)	119.5	22.7	–80.7	87.0	–0.25	21.0	–82.2	87.6	–0.24	16.1	–86.3	88.1	–0.02
	CERES (ocean)	81.8	110.5	35.1	110.8	0.01	112.6	37.6	112.0	–0.00	57.9	–29.2	83.7	0.14
AOD	MODIS (land)	0.15	0.16	1.5	22.4	0.53	0.16	1.5	22.9	0.53	0.16	3.5	22.7	0.54
	MODIS (ocean)	0.21	0.14	–34.6	34.9	0.34	0.14	–34.5	34.6	0.34	0.14	–31.5	32.2	0.29
CCN5 (10⁸ cm⁻²)	MODIS (ocean)	2.8	2.8	–0.8	42.5	–0.03	2.8	–0.7	42.7	–0.03	2.5	–12.7	40.3	0.07
CDNC	Bennartz (2007)	49.6	132.7	167.4	256.1	–0.09	138.9	179.8	253.7	–0.09	136.5	175.1	249.1	–0.08
PBLH (m)	NARR (land)	872.6	556.4	–36.2	36.2	0.40	553.4	–36.6	36.6	0.40	557.1	–36.2	36.2	0.41
	NARR (ocean)	530.0	615.9	16.2	26.0	0.24	614.7	16.0	25.8	0.24	513.4	–3.1	22.0	0.12
SST (°C)	OAFlux (ocean)	28.3	28.5	0.6	1.2	0.76	28.4	0.4	1.2	0.76	27.5	–2.8	3.8	0.63
LHFLX (W m⁻²)	NDBC	27.8	27.9	0.3	1.8	0.96	27.8	0.2	2.4	0.96	27.0	–2.9	4.8	0.78
	OAFlux (ocean)	111.6	178.7	60.1	60.2	0.72	179.4	60.7	60.8	0.72	132.7	18.9	26.9	0.47
SHFLX (W m⁻²)	OAFlux (ocean)	5.2	12.3	138.2	139.8	0.67	12.4	140.7	142.4	0.67	7.7	50.2	76.9	0.36

Table 2(b). Statistical Performance of Chemical Species.

Species/Variables	Datasets	obs	SEN1				SEN2				SEN3			
			sim	NMB (%)	NME (%)	Corr	sim	NMB (%)	NME (%)	Corr	sim	NMB (%)	NME (%)	Corr
CO	SEARCH	160	241.1	50.6	62.1	0.31	242.5	51.4	63.2	0.30	248.6	49.0	60.2	0.33
SO$_2$	CASTNET	1.2	3.6	204.5	219.4	0.31	3.6	201.1	205.6	0.33	3.4	192.1	207.1	0.33
NO$_2$	SEARCH	1.1	0.8	-23.0	101.9	0.08	0.9	-21.3	103.0	0.08	0.8	-23.8	102.5	0.06
HNO$_3$	SEARCH	4.2	5.3	23.6	100.9	0.45	5.4	26.9	104.6	0.43	5.2	23.4	100.1	0.45
	CASTNET	1.1	2.1	92.4	93.0	0.58	2.1	91.9	92.5	0.57	2.0	85.1	85.6	0.62
Max 1-h O$_3$	CASTNET	51.6	53.1	3.0	19.4	0.55	52.8	2.4	20.0	0.53	52.6	2.1	19.7	0.54
	AIRS-AQS	52.4	60.6	15.6	24.2	0.57	60.5	15.4	23.5	0.57	60.2	14.8	23.7	0.58
Max 8-h O$_3$	CASTNET	46.8	53.0	13.2	21.5	0.61	52.8	12.7	21.8	0.59	52.5	12.2	21.5	0.59
	AIRS-AQS	47.3	56.8	20.0	25.5	0.99	56.7	19.8	25.7	0.99	56.6	19.2	25.1	0.99
Hourly O$_3$	AIRS-AQS	31.7	40.3	27.3	41.4	0.68	40.2	27.1	41.4	0.68	40.0	26.4	40.7	0.69
	SEARCH	28.3	37.6	32.7	46.7	0.66	37.5	32.5	46.6	0.66	37.6	32.9	47.0	0.66
NH$_4^+$	STN	1.0	1.2	19.6	62.3	0.45	1.2	20.0	63.3	0.44	1.2	17.0	63.0	0.46
SO$_4^{2-}$	CASTNET	1.2	1.2	1.3	35.2	0.50	1.2	0.4	35.1	0.47	1.2	-1.6	34.0	0.51
	IMPROVE	3.1	2.9	-5.1	53.6	0.40	2.9	-5.1	52.3	0.41	2.9	-4.0	50.7	0.41
	STN	3.6	3.1	-13.9	51.5	0.38	3.1	-13.7	51.1	0.38	3.1	-13.6	52.3	0.34
NO$_3^-$	CASTNET	4.1	3.4	-15.6	31.1	0.43	3.4	-16.1	32.6	0.39	3.4	-17.2	31.5	0.42
	IMPROVE	0.3	0.4	63.3	138.8	0.23	0.4	62.3	140.1	0.19	0.4	48.6	124.7	0.31
	STN	0.4	0.7	61.6	128.3	0.26	0.7	63.5	131.7	0.21	0.6	51.0	120.7	0.22
	CASTNET	0.4	0.6	50.9	130.8	0.10	0.6	48.5	129.3	0.11	0.6	42.4	124.4	0.13
Na$^+$	IMPROVE	0.4	0.1	-68.8	73.8	0.39	0.1	-69.2	73.9	0.39	0.1	-69.0	73.4	0.40
Cl$^-$	IMPROVE	0.2	0.02	-86.0	88.0	0.57	0.02	-85.2	88.2	0.57	0.03	-83.7	85.4	0.66
EC	IMPROVE	0.3	0.4	43.0	81.1	0.29	0.4	42.2	80.6	0.28	0.4	40.4	79.1	0.27
	SEARCH	1.4	0.5	-63.1	75.9	0.48	0.5	-62.2	75.8	0.47	0.5	-63.3	75.8	0.49
OC	IMPROVE	1.5	1.9	30.0	66.4	0.40	1.9	28.9	66.0	0.38	1.9	30.3	63.2	0.41
	SEARCH	3.0	3.0	-0.4	67.7	0.15	3.0	0.5	68.6	0.15	3.0	-0.4	65.6	0.16
TC	STN	2.9	2.9	1.0	46.3	0.46	2.9	1.2	47.5	0.45	2.8	-2.6	46.1	0.45
	SEARCH	3.7	3.8	1.5	61.5	0.21	3.8	3.8	63.2	0.21	3.7	0.4	58.9	0.25
PM$_{2.5}$	IMPROVE	10.2	9.0	-12.0	40.5	0.31	9.0	-12.0	40.3	0.31	9.0	-11.8	39.0	0.33
	STN	14.1	10.6	-25.1	41.5	0.36	10.6	-25.0	41.3	0.36	10.3	-27.1	41.8	0.36
	SEARCH	8.6	10.2	19.1	91.8	-0.06	10.4	21.8	93.0	-0.06	10.3	20.6	89.8	-0.08
PM$_{10}$	AIRS-AQS	27.4	10.4	-62.1	66.8	0.13	10.4	-62.0	66.5	0.14	10.5	-61.7	66.3	0.13
Col.CO	MOPITT	1.8×10^{18}	2.6×10^{18}	50.7	50.7	0.81	2.6×10^{18}	50.8	50.8	0.80	2.6×10^{18}	50.8	50.8	0.80
Col.NO$_2$	SCIMACHY	1.3×10^{15}	3.0×10^{15}	129.0	129.2	0.79	3.0×10^{15}	129.0	129.3	0.79	3.0×10^{15}	132.2	132.4	0.78
Col. SO$_2$	SCIMACHY	0.27	0.10	-61.2	69.7	0.33	0.10	-61.4	69.8	0.33	0.10	-61.1	69.3	0.33
TOR	OMI/MLS	40.1	46.3	15.6	16.4	0.64	46.4	15.8	16.6	0.64	47.1	17.5	17.8	0.64
AOD	MODIS (land)	0.15	0.16	1.5	22.4	0.53	0.16	1.5	22.9	0.51	0.16	3.5	22.7	0.54
	MODIS (ocean)	0.21	0.14	-34.6	34.9	0.34	0.14	-34.5	34.6	0.35	0.14	-31.5	32.2	0.29

* The units for all surface gaseous and aerosol species are μg m^{-3} except for CO (ppb), SO$_2$ (ppb), NO$_2$ (ppb) against SEARCH, and O$_3$ (ppb). The units for column CO and NO$_2$ are molecules cm^{-2} and for column SO$_2$ and TOR are DU.

Environmental Information (NCEI, ftp://ftp.ncdc.noaa.gov/pub/data/noaa). Daily precipitation rate (Precip) is evaluated against estimations from the Global Precipitation Climatology Project (GPCP, http://www.esrl.noaa.gov/psd/data/gridded/data.gpcp.html) and the Multi-satellite Precipitation Analysis from the Tropical Rainfall Measuring Mission-Multi-satellite Precipitation Analysis (TMPA, http://disc.sci.gsfc.nasa.gov/gesNews/trmm_v7_multisat_precip). Radiative variables such as outgoing longwave radiation (OLR), downwelling shortwave radiation (SWD), downwelling longwave radiation (LWD), shortwave cloud forcing (SWCF), and longwave cloud forcing (LWCF) are evaluated against satellite retrievals from the Clouds and Earth's Radiant Energy System (CERES) Energy Balanced And Filled data product (CERES-EBAF, http://ceres.larc.nasa.gov/compare_products.php). Cloud properties such as cloud fraction (CF), cloud optical thickness (COT), and cloud liquid water path (LWP) are also evaluated against satellite retrievals from the CERES Synoptic product at 1° spatial resolution (CERES-SYN1deg, http://ceres.larc.nasa.gov/compare_products.php). Other related variables such as aerosol optical depth (AOD), precipitating water vapor (PWV), and cloud condensation nuclei at supersaturation of 0.5% (CCN5) are evaluated against satellite retrievals from the Moderate Resolution Imaging Spectroradiometer (MODIS, https://ladsweb.nascom.nasa.gov/data/search.html) and cloud droplet number concentration (CDNC) is evaluated against MODIS-derived CDNC from Bennartz (2007). Air-sea interaction related variables are evaluated including SST and WS10 from the National Data Buoy Center (NDBC, http://www.ndbc.noaa.gov/); PBLH derived from the National Centers for Environmental Prediction (NCEP)/North American Regional Reanalysis (NARR, http://www.esrl.noaa.gov/psd/data/gridded/data.narr.html); SST, sensible heat flux (SHFLX) and latent heat flux (LHFLX) derived

from the Objectively Analyzed Air-Sea Fluxes (OAFlux, http://oaflux.whoi.edu/dataproducts.html).

Surface chemical concentrations evaluated include O_3, sulfur dioxide (SO_2), nitric acid (HNO_3), particulate matter with diameter less and equal to 2.5 μm ($PM_{2.5}$) and 10 μm (PM_{10}), and $PM_{2.5}$ components such as sulfate (SO_4^{2-}), ammonium (NH_4^+), nitrate (NO_3^-), sodium (Na^+), chloride (Cl^-), elementary carbon (EC), and organic carbon (OC). These species are observed from various observational networks over southeastern U.S., such as the Clean Air Status and Trends Network (CASTNET), the Interagency Monitoring of Protected Visual Environments (IMPROVE), the Speciation Trends Network (STN), the Aerometric Information Retrieval System-Air Quality System (AIRS-AQS), and the Southeastern Aerosol Research and Characterization (SEARCH). The locations of these sites are plotted in Fig. 3. Column concentrations are evaluated over southeastern U.S., including tropospheric carbon monoxide (CO) retrieved from the Measurements Of Pollution In The Troposphere (MOPITT, https://www2.acom.ucar.edu/mopitt), tropospheric nitrogen dioxide (NO_2) retrieved from the SCanning Imaging Absorption spectroMeter for Atmospheric CHartographY (SCIAMACHY, http://www.sciamachy.org/), and tropospheric O_3 residual (TOR) retrieved from the Aura Ozone Monitoring Instrument in combination with Aura Microwave Limb Sounder (OMI/MLS, http://acdb-ext.gsfc.nasa.gov/Data_services/cloud_slice/new_data.html). The protocols for performance evaluation include spatial distributions and statistics, following the approach of Zhang *et al.* (2006, 2009). The analysis of the performance statistics focuses on mean bias (MB), normalized mean bias (NMB), normalized mean error (NME), root mean square error (RMSE), and correlation coefficient (Corr). The definitions of those statistics can be found in Yu *et al.* (2006) and Zhang *et al.* (2006).
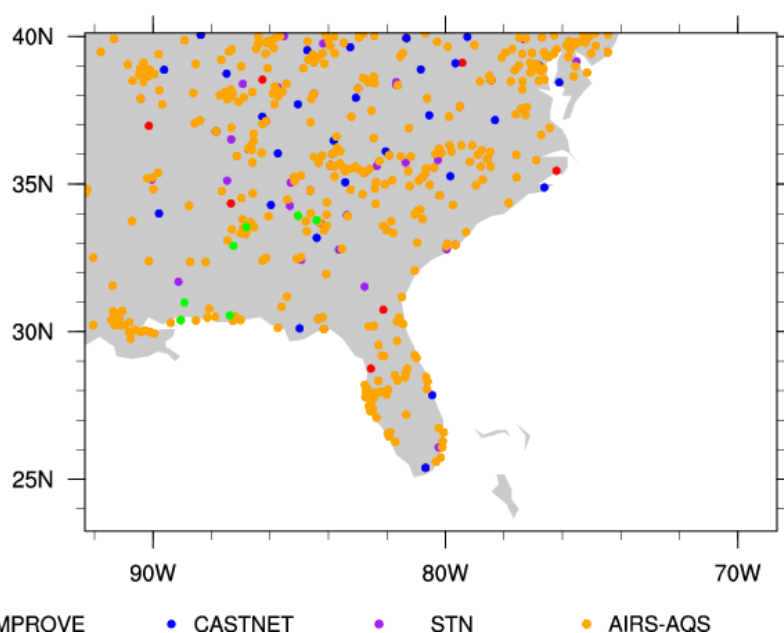

Fig. 3. Chemical observational sites including IMPROVE, CASTNET, STN, AIRS-AQS, and SEARCH in the study domain.

SIMULATION RESULTS AND EVALUATION

Impacts of 1-D Ocean Mixed Layer Coupling
Impacts on Meteorology

Fig. 4 shows the NMBs of model predictions for major meteorological and cloud variables (detailed statistics are shown in Table S1(a) in the supplementary material). As shown in Fig. 4, with the 1-D OML coupling in SEN2, the predictions of most meteorological, cloud, and radiative variables are comparable to SEN1. As shown in Table S1(a), the prescribed SSTs in SEN1 agree well with observations from OAFlux, with a mean bias of 0.2°C and an NMB of 0.6%. SST is well predicted in SEN2, with a mean bias of 0.1°C and an NMB of 0.4%. The RMSEs of SST against OAFlux are about 1.0°C in both SEN1 and SEN2. SEN1 is a forced simulation with prescribed SST from NCEP, whereas SST is prognostic in SEN2 with SST updated every model time step (i.e., 60 seconds) and every 10-min, respectively. However, the coupling with the 1-D OML causes very small changes in the simulated SST. The simulated SST from SEN2 is quite similar to those based on the NCEP reanalysis data. The 1-D OML model represents the cooling of SST due to deep mixing of the ocean layers below with stably stratified cooler water. The simplified representation of air-sea interaction in 1-D OML could leads to SST deviations. For example, the initial mixed layer depth (i.e., 50 m) and temperature lapse rate (i.e., 0.14 K m^{-1} are specified in the model for the entire domain, which is a main source of uncertainty considering the special heterogeneity.

Figs. 5(a) and 5(b) compare monthly-averaged satellite observations/reanalysis data with model predictions. As shown in Fig. 5(a), both SEN1 and SEN2 give warm SST bias for Gulf Stream, which can increase evaporation and convective instability. As a result, an atmospheric circulation that produces moisture convergence and convection occurs in response to SST gradients. Compared to NCEP/NARR reanalysis data, both SEN1 and SEN2 overpredict PBLH over ocean, with NMBs of 16.2%, and 16.0%, respectively. The biases in PBLH can be due in part to different methods for calculating PBLH in the NCEP models (e.g., the Global Forecast System and North American Model) and WRF. Also, Seidel *et al.* (2012) found that the NCEP reanalysis data showed deeper PBLH due to difficulty in simulating stable conditions compared with radiosonde observations. Therefore, the performance of PBLH here can only represent the deviation from the NCEP models. LHFLX is largely overpredicted in both SEN1 and SEN2, with NMBs of 60.1% and 60.7%, respectively. Similarly, SHFLX (Figure not
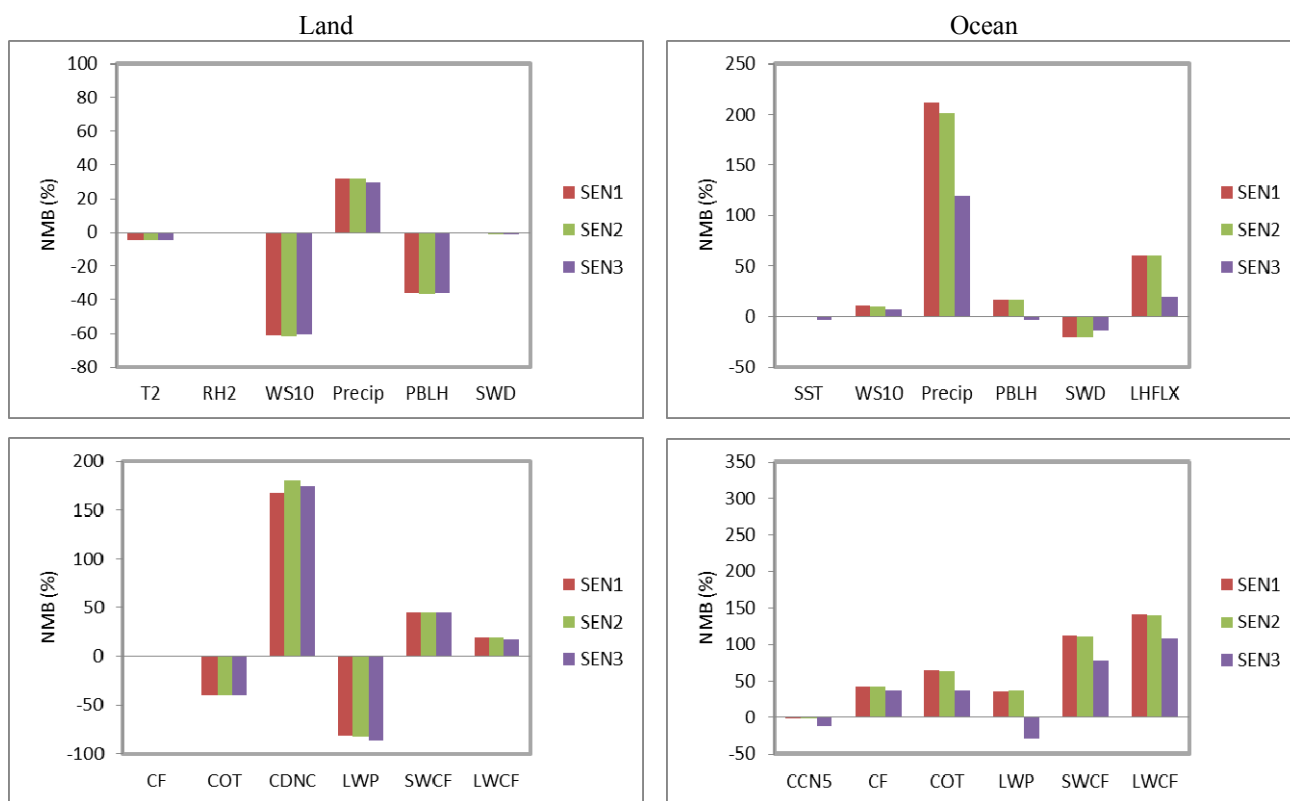

Fig. 4. The normalized mean bias (NMB, %) of major meteorological and cloud variables from SEN1 (WRF/Chem standalone without coupling ocean model), SEN2 (WRF/Chem coupling with 1-D ocean mixing layer model), and SEN3 (WRF/Chem coupling with 3-D ROMS) over land (left column) and ocean (right column). T2: temperature at 2-m; RH2: relative humidity at 2-m; WS10: wind speed at 10-m, Precip: daily precipitation rate; PBLH: planetary boundary layer height; SWD: downwelling shortwave radiation; SST: sea surface temperature; LHFLX: latent heat flux; CF: cloud fraction; COT: cloud optical thickness; CDNC: cloud droplet number concentration; LWP: cloud liquid water path; SWCF: shortwave cloud forcing; LWCF: longwave cloud forcing; CCN5: cloud condensation nuclei at supersaturation of 0.5% (CCN5).
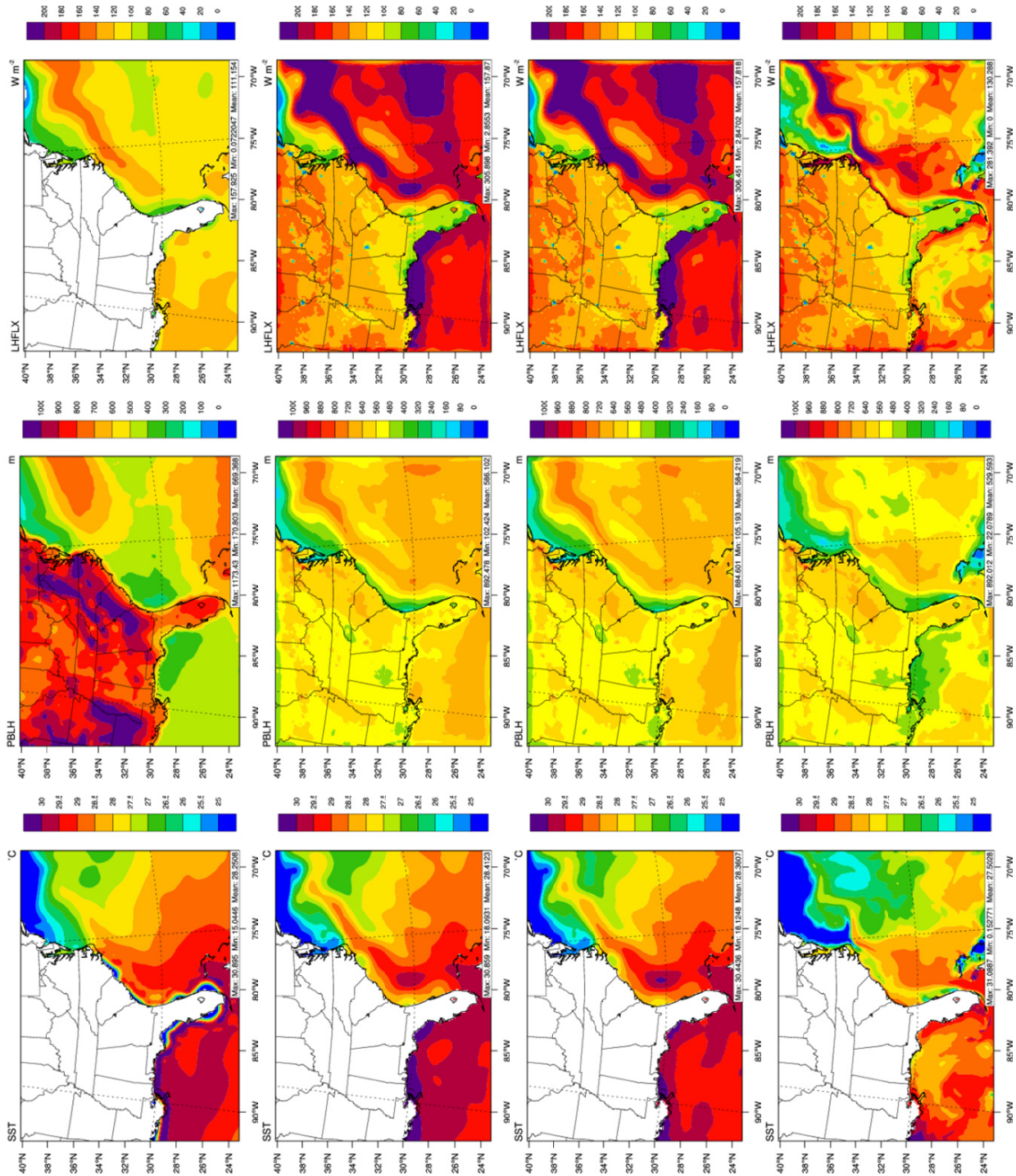
Fig. 5(a). Comparison of satellite observations/reanalysis data (row 1) with monthly-averaged predictions of for SST, PBLH, and LHFLX by SEN1 (WRF/Chem standalone without coupling ocean model, row 2), SEN2 (WRF/Chem coupling with 1-D ocean mixed layer model, row 3), and SEN3 (WRF/Chem coupling with 3-D ROMS, row 4).
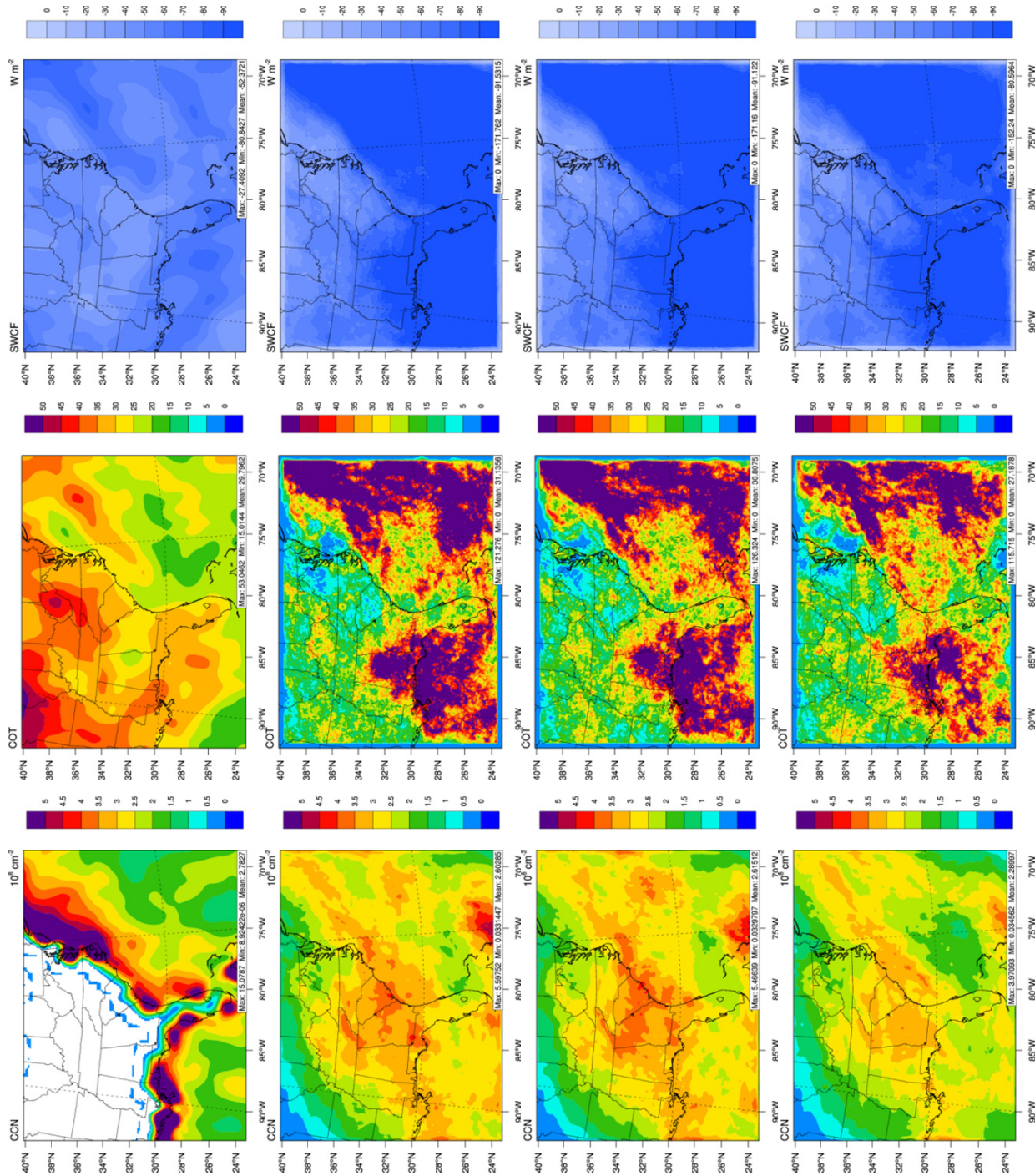
Fig. 5(b). Comparison of satellite observations (row 1) with monthly-averaged predictions of for CCN, COT, and SWCF by SEN1 (WRF/Chem standalone without coupling ocean model, row 2), SEN2 (WRF/Chem coupling with 1-D ocean mixed layer model, row 3), and SEN3 (WRF/Chem coupling with 3-D ROMS, row 4).

shown) is also largely overpredicted in both SEN1 and SEN2, with NMBs of 138.2% and 140.7%, respectively. The large over predictions in LHFLX and SHFLX are associated with the large differences in specific humidity and temperature between atmosphere and ocean interface predicted in SEN1 and SEN2. Due to the simplified assumptions and treatments in 1-D OML, the impacts on SWD is small, with a domain average of decrease by 0.5 W m^{-2}.

Compared to GPCP data, precipitation is largely overpredicted over ocean in both SEN1 and SEN2, with NMBs of 211.5% and 210.3%, respectively. The overpredictions of precipitation over ocean are likely due in part to the uncertainties in the convective precipitation associated with the cumulus scheme (He *et al.*, 2017) and the satellite retrievals. Due to the limited impacts of 1-D OML on meteorology, the impacts on clouds are also very small. The predictions of most cloud variables are comparable in SEN1 and SEN2 as shown in Figs. 4 and 5(b). Both SEN1 and SEN2 underpredict cloud variables such as COT and LWP over land, possibly due to less cloud formed in the model, which is common in the applications of WRF reported in previous studies (e.g., Wang *et al.*, 2015a; Thompson *et al.*, 2016). Meanwhile, both SEN1 and SEN2 overpredict COT and LWP over ocean, due in part to more cloud formed in the model. The overpredictions of CDNC by both SEN1 and SEN2 are not well representative in this work, since there are only a few grid cells in the MODIS-derived CDNC data that contain valid observations.

Impacts on Atmospheric Pollutants

Fig. 6 shows the absolute differences between SEN2 and SEN1 for monthly-averaged surface chemical predictions. The results from SEN1 are shown in Fig. S3. With 1-D OML model, the changes of most surface chemical species are small. For example, the differences in surface CO mixing ratios between SEN2 and SEN1 are within 11 ppb (or within 3%). The absolute differences in surface mixing ratios of SO_2, NO_2, and O_3 are within 2 ppb, and the percentage differences can be as large as 29.8%, 14.4%, and 6.5%, respectively. Although the absolute differences in surface concentrations of SO_4^{2-}, SOA, sea-salt, $PM_{2.5}$, and PM_{10} are within 1.5 µg m^{-3}, the percentage differences can be as large as 20.2%, 757.5%, 48.6%, 9.0%, and 11.7%, respectively. The large value of 757.5% by SOA is caused by very low SOA concentration predicted in the model. Therefore, a small change in SOA concentration can lead to a large percentage difference. The relatively large change of SOA concentrations up to 0.4 µg m^{-3} in SEN2 is likely due to higher OH levels (Figure not shown) and lower PBLH over southeastern domain (e.g., 31–34°N).

Impacts of 3-D Ocean Model Coupling
Impacts on Meteorology

As shown in Figs. 5(a) and 5(b), unlike the small impacts on model predictions with the 1-D OML coupling, the impacts with atmosphere-ocean coupling by SEN3 affect boundary layer properties more significantly. As shown in Fig. 4 and Table S1(a), SST is slightly underpredicted in SEN3, with an NMB of –2.8%, and a RMSE of 1.5°C in

SEN3, with a larger cold bias than the warm biases in SEN1 and SEN2. The cold bias for SST in SEN3 can be attributed in part to the lower ICs and BCs from HYCOM-NCODA, and in part to the use of a coarse vertical resolution in the ocean layers used in HYCOM (Hofmeister *et al.*, 2010; Shapiro *et al.*, 2013) and ROMS, as well as possible weak southward currents from ROMS. A comparison of SST predictions from HYCOM with satellite retrievals indicates lower values from this model, especially near the coast, due likely to the inherent uncertainties in the model setting (e.g., the surface layer depth used for SST calculation is larger in the simulations at a coarse grid resolution than at a fine grid resolution). For example, Bernie *et al.* (2005) found that 90% of the observed diurnal SST can be captured by high temporal and vertical resolutions (e.g., the vertical resolution of 1-m in the upper ocean and the temporal resolution of more than 3-h for surface fluxes). In addition, the poor representation of the Gulf Stream and North Atlantic Current in the ocean models (e.g., Willebrand *et al.*, 2001; Eden *et al.*, 2004) can also contribute to the biases in SST.

Compared to NCEP/NARR reanalysis data, SEN3 predicts PBLH well, with an NMB of –3.1%. The decreases in PBLH in SEN3 compared to SEN1 are associated with lower SST, which results in less evaporation and less convective instability. Therefore, the boundary layer is more stable predicted by SEN3 than SEN1. LHFLX depends on the difference in sea-air specific humidity (i.e., $Q_s - Q_a$). Since Q_a in SEN3 is lower than that in SEN1 over ocean, and Q_s is SST-dependent, the LHFLX-SST correlation is positive, suggesting the dominance of oceanic forcing (i.e., the decrease of Q_s due to the changes in SST is dominant) of atmosphere in the western Atlantic Ocean. The significant differences of WS10 between SEN3 and SEN1 (Figure not shown) are mainly over open ocean and Gulf of Mexico, with a domain average of –0.2 m s^{-1} up to –2.1 m s^{-1}, which is mainly attributed to changes induced by SST. Cold water surface increases atmospheric stability, which decouples the surface winds from the stronger winds aloft and reduces surface wind speed. Due to all above changes, compared to SEN1, SEN3 predicts lower LHFLX with a domain averaged decrease of 27.8 W m^{-2}. With the coupling of 3-D ocean model, SWD increases with a domain average of 9.7 W m^{-2}. The increases of SWD in SEN3 are mainly due to reduced cloud fractions (mainly over ocean) through impacts of air-sea interactions. For example, colder SST in SEN3 leads to less evaporation and therefore less moisture available for cloud formation. As a result, the predictions of SWD are improved, with an NMB of –20.6% by SEN1 to –13.7% by SEN3.

Compared to GPCP data, total precipitation is still largely overpredicted over ocean in SEN3, but is significantly improved, with an NMB reducing from 211.5% (in SEN1) to 119.2% (in SEN3). Compared to TMPA data, total precipitation is moderately overpredicted over ocean in SEN3, with an NMB of 60.6%. The lower precipitation in SEN3 than SEN1 is probably due to the changes in moisture flux convergence through large-scale changes in the circulation field and SST predicted by ROMS (Keeley *et al.*, 2012). The overpredictions of total precipitation
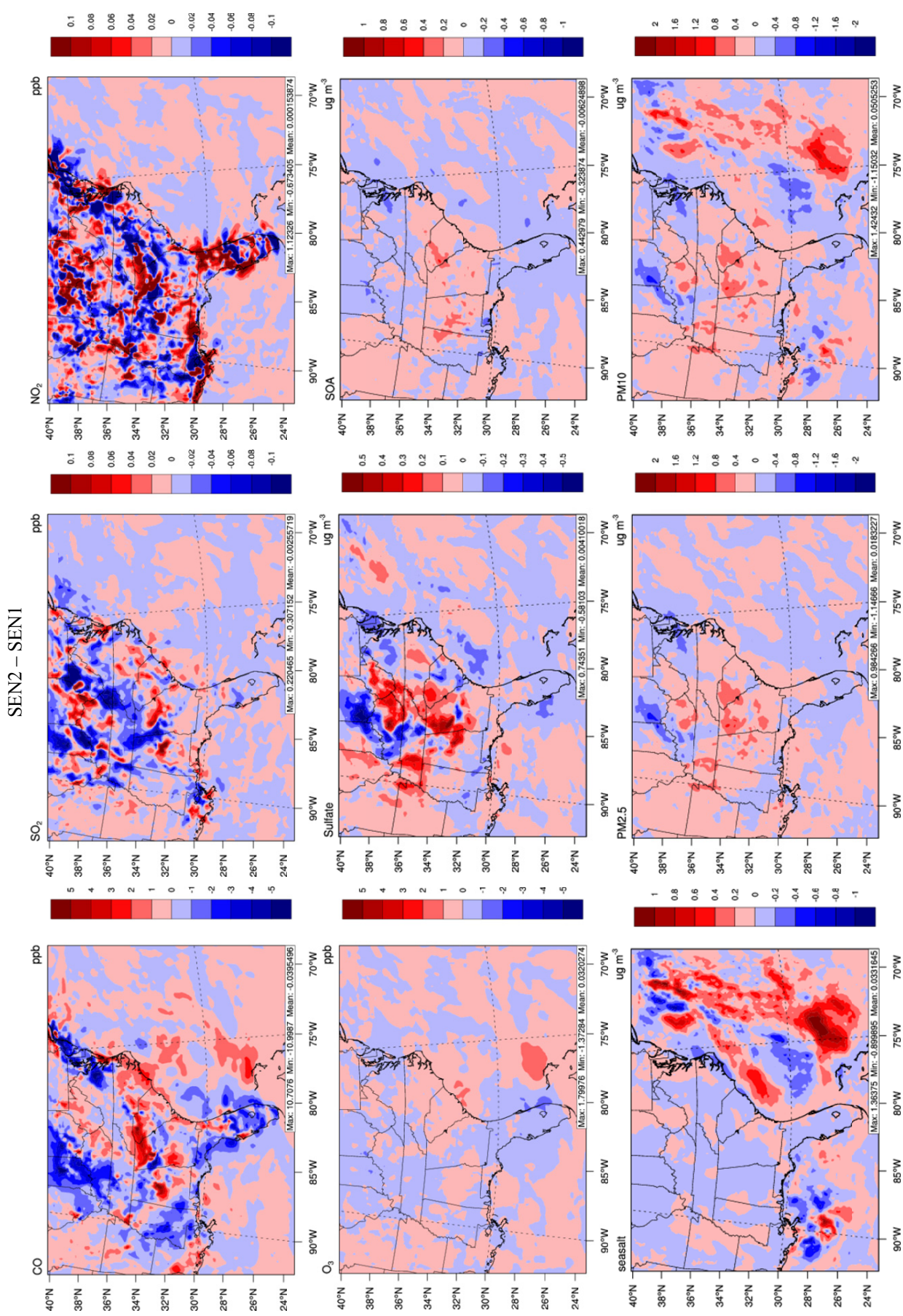
Fig. 6. Absolute differences in the monthly-averaged predictions of surface concentrations of chemical species between SEN2 (WRF/Chem coupling with 1-D ocean mixed layer model) and SEN1 (WRF/Chem standalone without ocean coupling).

over ocean are likely due in part to the uncertainties in the convective precipitation associated with the restoration stability (He *et al.*, 2017) and the satellite retrievals. Detailed model statistics can be found in Table S1(a) in the supplementary material.

Impacts on Clouds

Unlike the comparable model predictions for most cloud variables between SEN1 and SEN2, SEN3 improves substantially the model's performance for the predictions of most cloud variables, especially over ocean. As shown in Fig. 5(b), compared to SEN1, monthly-averaged column concentration of CCN5 is lower in SEN3 over most domain, with a domain averaged decrease of 3.0×10^{-7} cm^{-2}. Compared to MODIS data, column concentration of CCN5 over ocean is underpredicted by both SEN1 and SEN3, with NMBs of –0.8% and –12.7%, respectively. The underpredictions of CCN5 are likely due to the inaccurate predictions of aerosol number concentrations, and uncertainties in the cloud thermodynamics. Compared to SEN1, SEN3 predicts higher COT up to 62.2, and lower COT up to 87.4, with a domain averaged decrease of 4.2. Compared to satellite data, both SEN1 and SEN3 underpredict COT over land, with NMBs of –39.5% and –39.8%, respectively, and they overpredict COT over ocean, with NMBs of 64.6% and 37.5%, respectively. The biases in COT predictions are likely due to the model uncertainties in cloud dynamics and thermodynamics, aerosol-cloud interactions, as well as satellite retrievals. Compared to SEN1, SEN3 predicts higher SWCF up to 21.0 W m^{-2} over land, and lower SWCF up to 77.9 W m^{-2} over ocean, with a domain averaged decrease of 11.4 W m^{-2}. The decrease of SWCF in SEN3 is mainly due to the decreases of COT and LWP in SEN3. Compared to satellite data, the prediction of SWCF is improved over ocean significantly, with NMBs from 112.5% in SEN1 to 78.5% in SEN3.

Other cloud/radiative variables are also improved over ocean. For example, CF is improved over ocean, with NMBs from 42.3% in SEN1 to 36.7% in SEN3. The decreases in CF by SEN3 are mainly due to less available moisture for cloud formation through air-sea interactions. As a result, LWP also decreases (especially over ocean), with NMBs from 35.1% in SEN1 to –29.2% in SEN3. Due to the improved cloud predictions, the performance of most radiative variables in SEN3 is also improved over ocean. For example, the prediction of SWD is improved over ocean with NMBs from –20.6% in SEN1 to –13.7% in SEN3. Predictions of OLR and LWCF are improved over ocean as well, with NMBs reduced from –20.7% in SEN1 to –16.8% in SEN3, and from 141.4% in SEN1 to 107.7% in SEN3, respectively. A detailed model statistical performance can be found in Table S1a in the supplementary material.

Impacts on Atmospheric Pollutants

Fig. 7 shows the absolute differences between SEN3 and SEN1 for monthly-averaged surface chemical predictions. With the coupling of 3-D ROMS, the changes in the concentrations of most surface chemical species in SEN3 are much larger than with coupling of 1-D OML in SEN2,

relatively to SEN 1. For example, surface CO mixing ratios can increase as large as 196.5 ppb and decrease as large as 304.9 ppb. Although the absolute differences in the surface mixing ratios of SO$_2$ and OH between SEN1 and SEN3 are within 1.5 ppb, the percentage differences in the surface mixing ratios of SO$_2$ and OH can be as large as 134.4% and 83.6%, respectively. The changes of the surface mixing ratios of NO$_2$ and O$_3$ are also significant, which can be as large as 18.0 ppb (or 189.2%) and 17.3 ppb (or 44.8%), respectively. The decreases of the mixing ratios of CO, SO$_2$, and NO$_2$ are likely due in part to the enhanced oxidation with higher OH concentrations in SEN3. The increase in OH concentrations can be attributed to the decrease of precipitation and PBLH, and the increase of SWD in SEN3. Compared to SEN1, surface SO$_4^{2-}$ concentrations predicted by SEN3 can increase as large as 0.9 µg m^{-3} and decrease as large as 1.2 µg m^{-3}. The changes in surface SO$_4^{2-}$ predictions are mainly due in part to changes in the mixing ratios of SO$_2$ and OH through gas-phase oxidation, changes in cloud fraction through aqueous-phase chemistry, and changes in precipitation (e.g., intensity and duration). Surface SOA predicted by SEN3 can increase as large as 0.7 µg m^{-3} and decrease as large as 1.5 µg m^{-3}. The changes in SOA predictions are likely due to the combined changes in OH mixing ratios, precipitation, SWD, and PBLH. There are similar patterns in changes of surface concentrations of PM$_{2.5}$ and PM$_{10}$ over land. Both PM$_{2.5}$ and PM$_{10}$ increase over 30–33°N, and decrease over 33–40°N. The increase of PM$_{2.5}$ can be as large as 3.0 µg m^{-3} and the decrease of PM$_{2.5}$ can be as large as 7.9 µg m^{-3}. The changes of PM$_{2.5}$ over land are mainly due to the changes in SO$_4^{2-}$, NH$_4^+$, and SOA, which can be attributed to the changes in precipitation and PBLH over land, and the changes of PM$_{2.5}$ over ocean are mainly due to the changes in SO$_4^{2-}$, NH$_4^+$, NO$_3^-$, SOA, and sea-salt, which can be attributed to the combined effects of changes in precipitation, PBLH, and WS10. The decreases of PM$_{10}$ over remote ocean are mainly due the decreases in sea-salt predictions resulted from lower WS10 in SEN3 than SEN1. As shown in Fig. 7, the most significant changes in surface chemical predictions are along coast, over remote ocean, and part of inland regions, indicating the significant impacts of air-sea interactions on air quality. The changes in surface chemical predictions over inland regions are mainly caused by the changes in meteorology (e.g., T2, PBLH, WS10, WD10, SWD, and precipitation) over these regions resulted from the coupling of ROMS with WRF/Chem.

The student's t-tests are also conducted for differences in monthly-averaged surface O$_3$ and PM$_{2.5}$ between SEN3 and SEN1, which is shown in Fig. 8. For changes in surface O$_3$, the differences are statistically significant over land where the absolute changes are larger than 2 ppb, along or near the coast (e.g., eastern Florida coast and Gulf coast) where the absolute changes are larger than 1 ppb, and over most oceanic areas (e.g., western Atlantic Ocean). The changes in surface O$_3$ mixing ratios are directly related to the changes in surface and boundary layer properties, which are impacted through coupling of air-sea interactions. The impacts from coupling ROMS with WRF-Chem are nonlinear
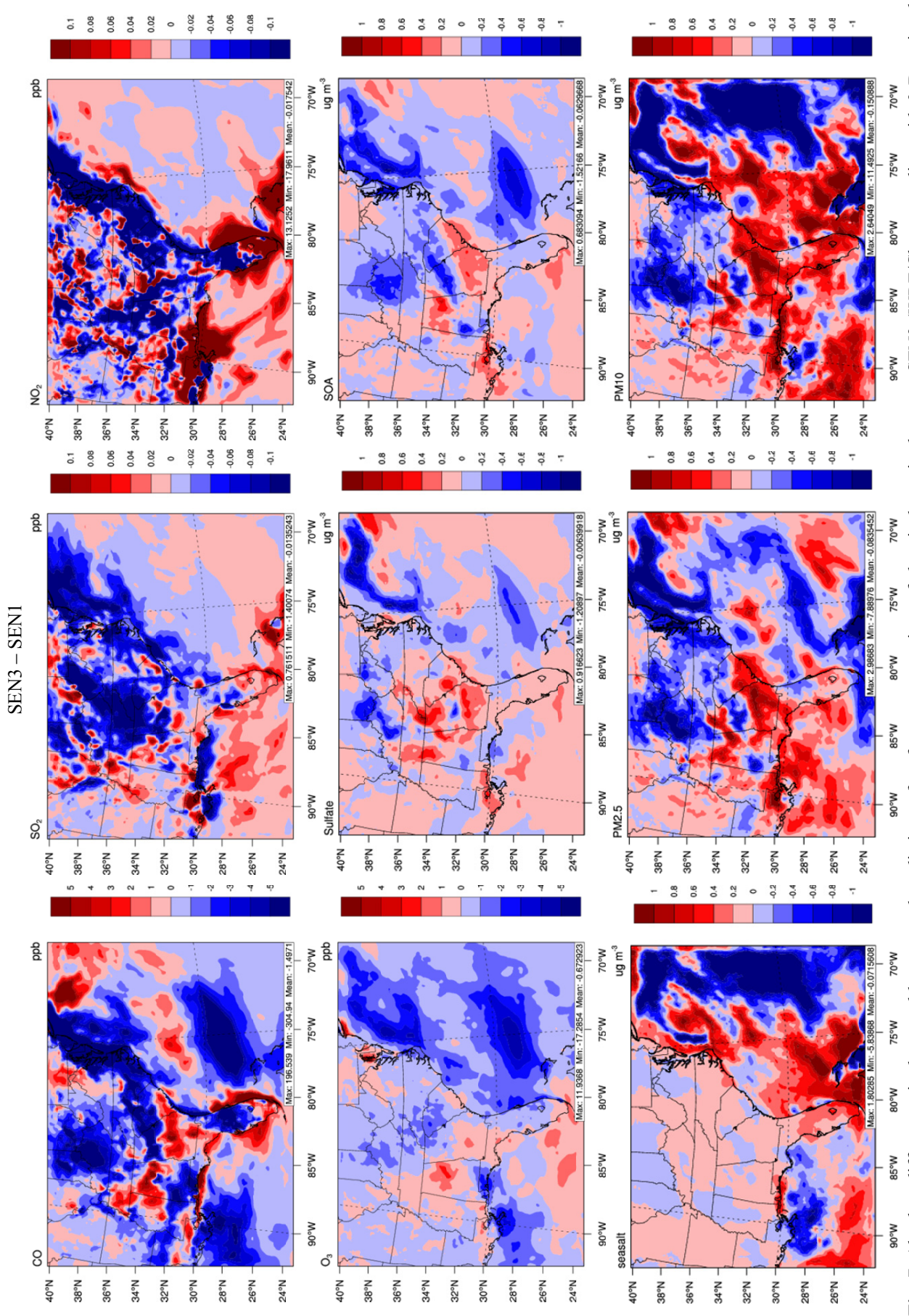
Fig. 7. Absolute differences in the monthly-averaged predictions of surface concentrations of chemical species between SEN3 (WRF/Chem coupling with 3-D regional ocean model) and SEN1 (WRF/Chem standalone without ocean coupling).
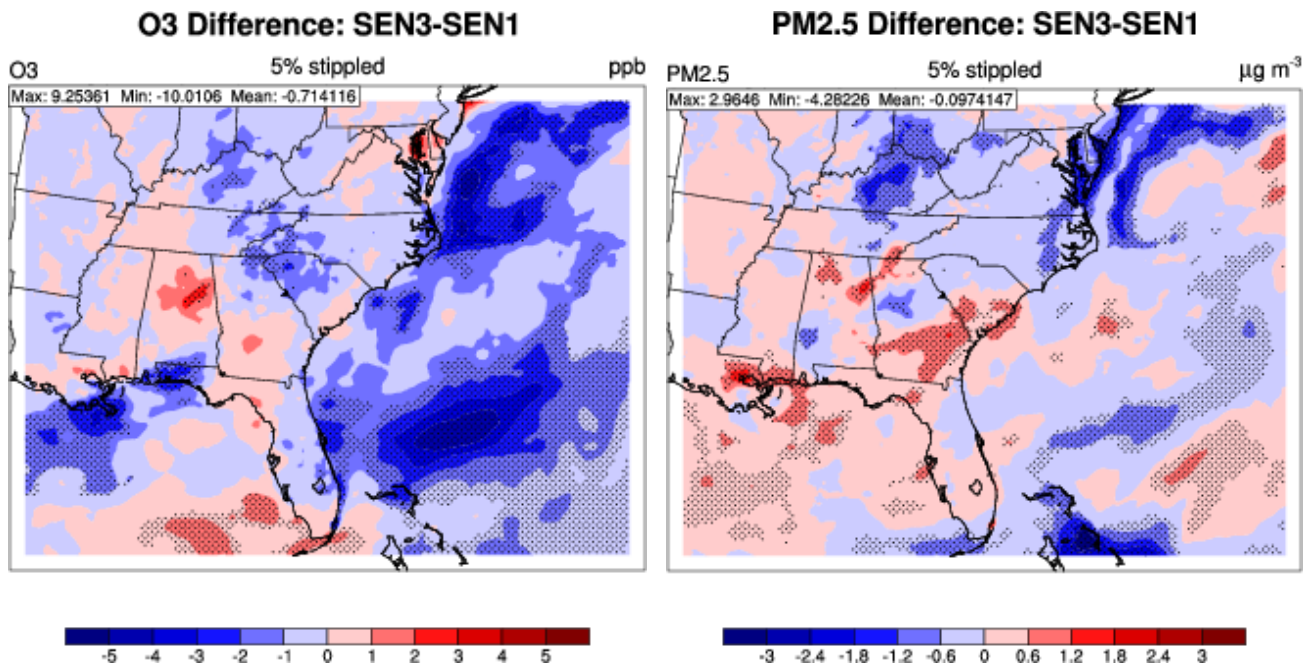
Fig. 8. Student's t-test for differences in monthly-averaged surface concentrations of O_3 and $PM_{2.5}$ between SEN3 (WRF/Chem coupling with 3-D regional ocean model) and SEN1 (WRF/Chem standalone without ocean coupling). The shaded areas indicate the differences are statistically significant at the confidence level of 95%.

and complex. For example, the significant decreases in surface O_3 concentration (e.g., > 5 ppb) over western Atlantic Ocean are likely due to the changes in turbulent fluxes, driven by differences in temperature and humidity between air and sea interfaces through coupling air-sea interactions. In addition, the impacts of air-sea interactions on meteorology can also affect O_3 concentrations through chemical transformation (e.g., photochemical oxidation, nighttime chemistry, and other kinetic reactions) and physical processes (e.g., deposition and transport). For example, changes in shortwave radiation induced by coupling air-sea interaction can affect the photolysis of NO_2, which is a major O_3 precursor. Changes in temperature and humidity can affect O_3 involved kinetic reactions (e.g., the reaction of volatile organic compounds with O_3). For changes in surface $PM_{2.5}$, the differences are statistically significant over land where the monthly mean absolute changes are larger than 1 µg m^{-3}, along or near the coast (e.g., Gulf coast and northeast coast) where the absolute changes are larger than 1 µg m^{-3}, and over remote oceanic area (e.g., middle Atlantic Ocean). Similar to changes in surface O_3, the changes in surface $PM_{2.5}$ are also driven by the changes in chemical, dynamic, and thermodynamics processes through air-sea interactions. Changes in surface temperature and radiation can result in changes in secondary aerosol formation. For example, the temperature-dependent reaction of SO_2 with OH can produce H_2SO_4 and therefore sulfate in the particulate phase. Changes in radiation can lead to changes in predicted OH radical, which can affect the formation of secondary organic aerosol. Changes in large-scale circulation can lead to horizontal transport of gases and aerosols. In addition, changes in precipitation can also affect PM concentrations through wet scavenging. These results indicate clearly the

impacts from coupling ROMS with WRF-Chem.

Figs. 9(a) and 9(b) show the time series observations and model predictions over coastal sites from CASTNET, IMPROVE, and AIRS-AQS for surface max 8-h mixing ratios of O_3 and 3-day averaged $PM_{2.5}$. Compared to SEN1, the differences in Max 8-h O_3 can be as large as about 15 ppb at the CASTNET sites. Max 8-h O_3 mixing ratios predicted by SEN1, SEN2, and SEN3 overall correlate well with observations at the CASTNET sites, with a better performance by SEN3 at sites BFT142 and IRL141. Compared to SEN1, the differences in Max 8-h O_3 mixing ratios can be as large as about 20 ppb at the AQS sites. Max 8-h O_3 mixing ratios by SEN3 are large overpredicted by three simulations at the AQS sites such as Holiday, FL (121012001) and Gulfport Youth Court, MS (280470008). Due to the relatively coarse grid resolution used in this work, the model shows some difficulties in capturing the observed temporal variations of O_3 during some time periods at some sites (e.g., overpredictions at Holiday, FL during most days, and at Gulfport Youth Court after July 15). However, compared to SEN1, SEN3 can capture temporal variations of max 8-h O_3 much better especially at Beaufort (BFT142) and Indian River Lagoon (IRL141) sites (e.g., from July 16 to Jul 31, 2010). As shown in Fig. 9(b), $PM_{2.5}$ is overall well predicted at the IMPROVE and AQS sites. Compared to SEN1, the differences in surface $PM_{2.5}$ predictions by SEN3 can be as large as about 15 µg m^{-3} at the IMPROVE sites and as large as about 6 µg m^{-3} at the AQS sites. In general, SEN3 predicts better magnitudes and temporal variations of $PM_{2.5}$ concentrations compared to SEN1, especially at the four sites: CHAS1, ROMA1, EVER1, and SWAN1.

Fig. 10 shows the scatter plots for major chemical species over various observational networks. Compared to
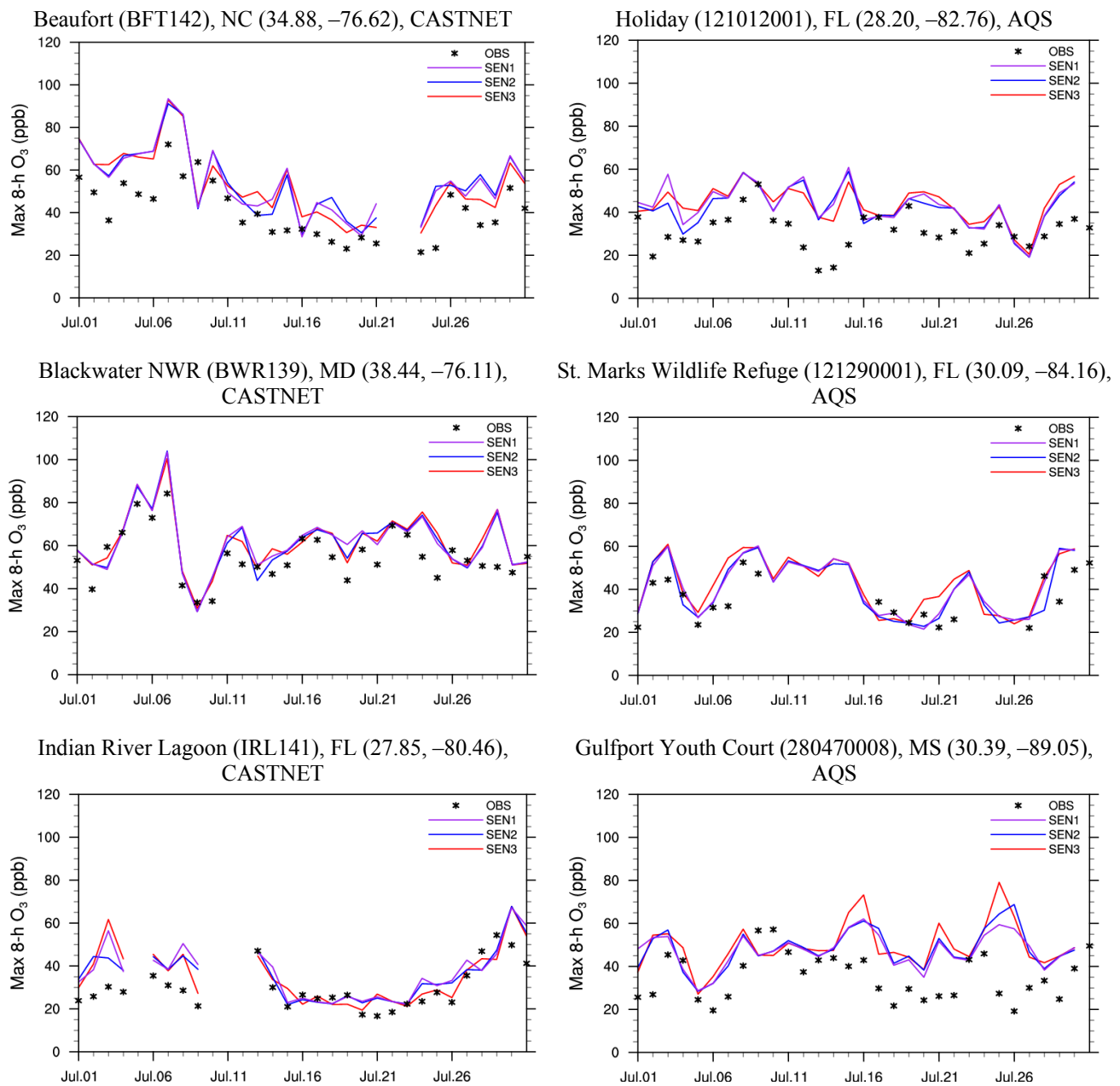
Beaufort (BFT142), NC (34.88, −76.62), CASTNET

Holiday (121012001), FL (28.20, −82.76), AQS

Blackwater NWR (BWR139), MD (38.44, −76.11), CASTNET

St. Marks Wildlife Refuge (121290001), FL (30.09, −84.16), AQS

Indian River Lagoon (IRL141), FL (27.85, −80.46), CASTNET

Gulfport Youth Court (280470008), MS (30.39, −89.05), AQS

Fig. 9(a). Maximum 8-h O_3 at 6 sites, including 3 from CASTNET, and 3 from AIRS-AQS. The black markers represent observations. The purple, blue, and red lines represent simulated results from SEN1 (WRF/Chem standalone without coupling ocean model), SEN2 (WRF/Chem coupling with 1-D ocean mixed layer model), and SEN3 (WRF/Chem coupling with 3-D ROMS), respectively.

SEN1, SEN3 predicts overall better chemical concentrations in terms of both NMB and R values. For example, the surface predictions of gaseous species such as SO_2 and HNO_3 are improved by reducing NMBs from 204.5% to 192.1%, and from 92.4% to 85.1%, respectively. The hourly O_3 prediction is slightly improved by reducing NMBs from 27.3% to 26.4% at the AIRS-AQS sites. The predictions of max 1-h and 8-h O_3 mixing ratios are also improved by reducing NMBs from 3.0% to 2.1% against CASTNET (from 15.6% to 14.8% against AIRS-AQS), and from 13.2% to 12.2% against CASTNET (20.0 to 19.2% against AIRS-AQS), respectively. Model predictions of aerosol species

such as SO_4^{2-}, NH_4^+, and NO_3^- are slightly or moderately improved against STN observations. The concentrations of Na^+ and Cl^- are largely underpredicted in both SEN1 and SEN3, indicating the uncertainties in the online sea-salt emission modules. In SEN3, the model performance of EC is slightly improved at the IMPROVE sites but slightly degraded at the SEARCH sites, whereas the model performance of OC and TC is slightly degraded at the IMPROVE sites but slightly improved at the SEARCH sites. $PM_{2.5}$ prediction is slightly improved in SEN3 at the IMPROVE sites, but degraded at the STN sites. PM_{10} prediction is also slightly improved in SEN3. The large

Chassahowitzka (CHAS1), FL (28.75, –82.56), IMPROVE

Everglades (EVER1), FL (25.39, –80.68), IMPROVE

Brigantine (BRIG1), NJ (39.47, –74.45), IMPROVE

St. Marks (SAMA1), FL (30.09, –84.16), IMPROVE

Cape Romain (ROMA1), SC (32.94, –79.66), IMRPOVE
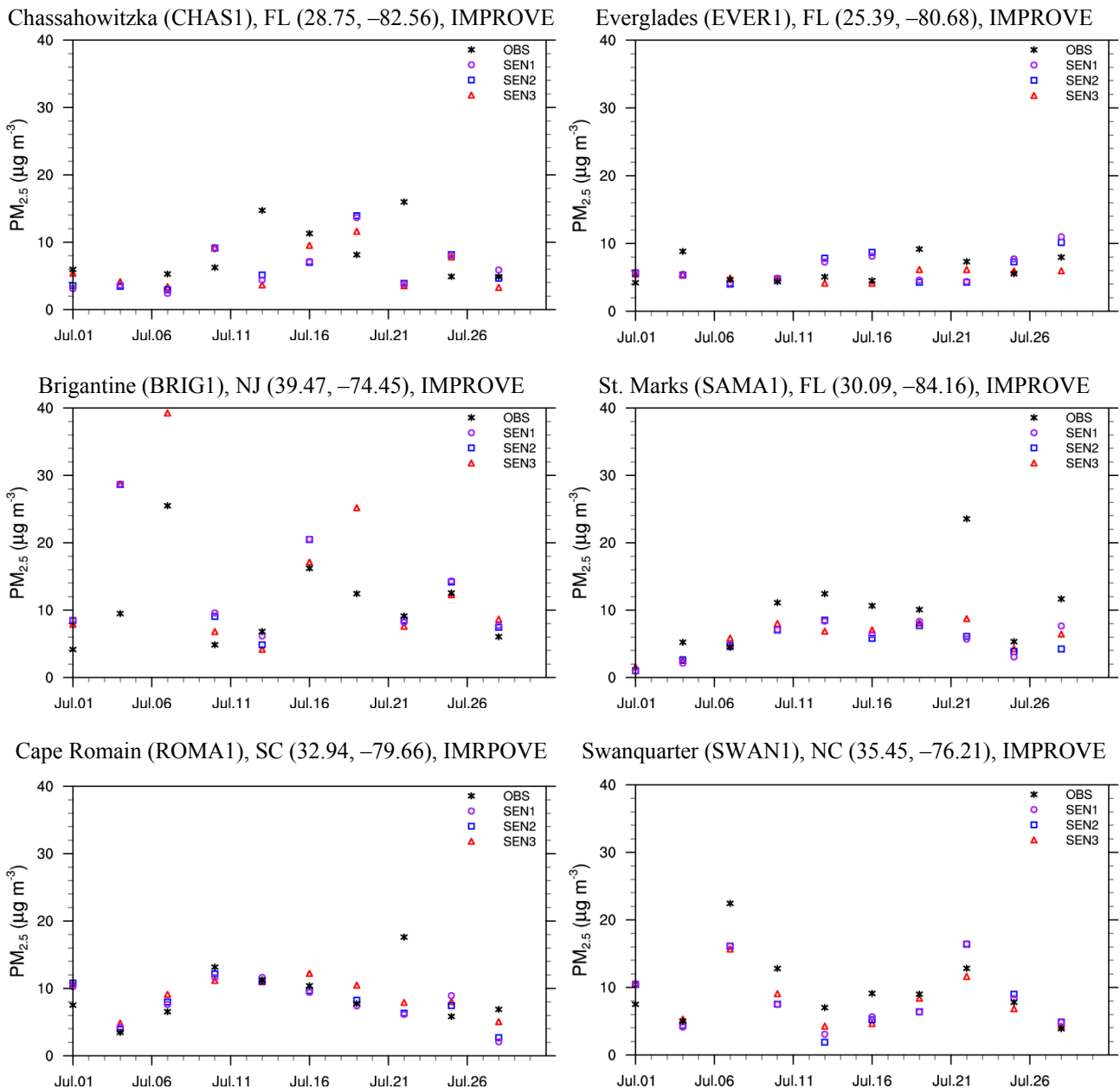
Swanquarter (SWAN1), NC (35.45, –76.21), IMPROVE

Fig. 9(b). Three-day averaged surface $PM_{2.5}$ concentrations at 6 sites from IMRPOVE. The black markers represent observations. The purple, blue, and red markers represent simulated results from SEN1 (WRF/Chem standalone without coupling ocean model), SEN2 (WRF/Chem coupling with 1-D ocean mixed layer model), and SEN3 (WRF/Chem coupling with 3-D ROMS), respectively.

underpredictions of PM_{10} are likely due to the inaccurate predictions of sea-salt concentrations and the overpredictions of precipitation over land (e.g., intensity and duration).

The model performance for column concentrations and AOD predictions is shown in Fig. 11. The predicted column concentrations of NO_2, CO, SO_2, and TOR are comparable in SEN1 and SEN3. The coupling of WRF/Chem with ROMS affects boundary layer more significantly than upper layers. As shown in Fig. 11, TOR is reasonably predicted by SEN1 and SEN3, with NMBs of 15.6%, and 17.5%, respectively. However, both SEN1 and SEN3 simulations moderately or largely overpredict column CO and NO_2.

Unlike the predictions of column CO and NO_2, column SO_2 is largely underpredicted by SEN1 and SEN3, with NMBs of –61.2% and –61.1%, respectively. The inaccurate predictions of total column of CO, NO_2, and SO_2 could be mainly attributed to the uncertainties in the total CO, NO_x, and SO_2 emissions, vertical distributions of emissions, as well as chemical reactions affecting those species. Compared to SEN1, SEN3 predicts slightly higher AOD up to 0.038, and slightly lower AOD up to 0.048. The higher AOD can be attributed to the higher aerosol concentrations due to less wet deposition in SEN3 since precipitation reduces largely in SEN3. Compared to MODIS data, both SEN1
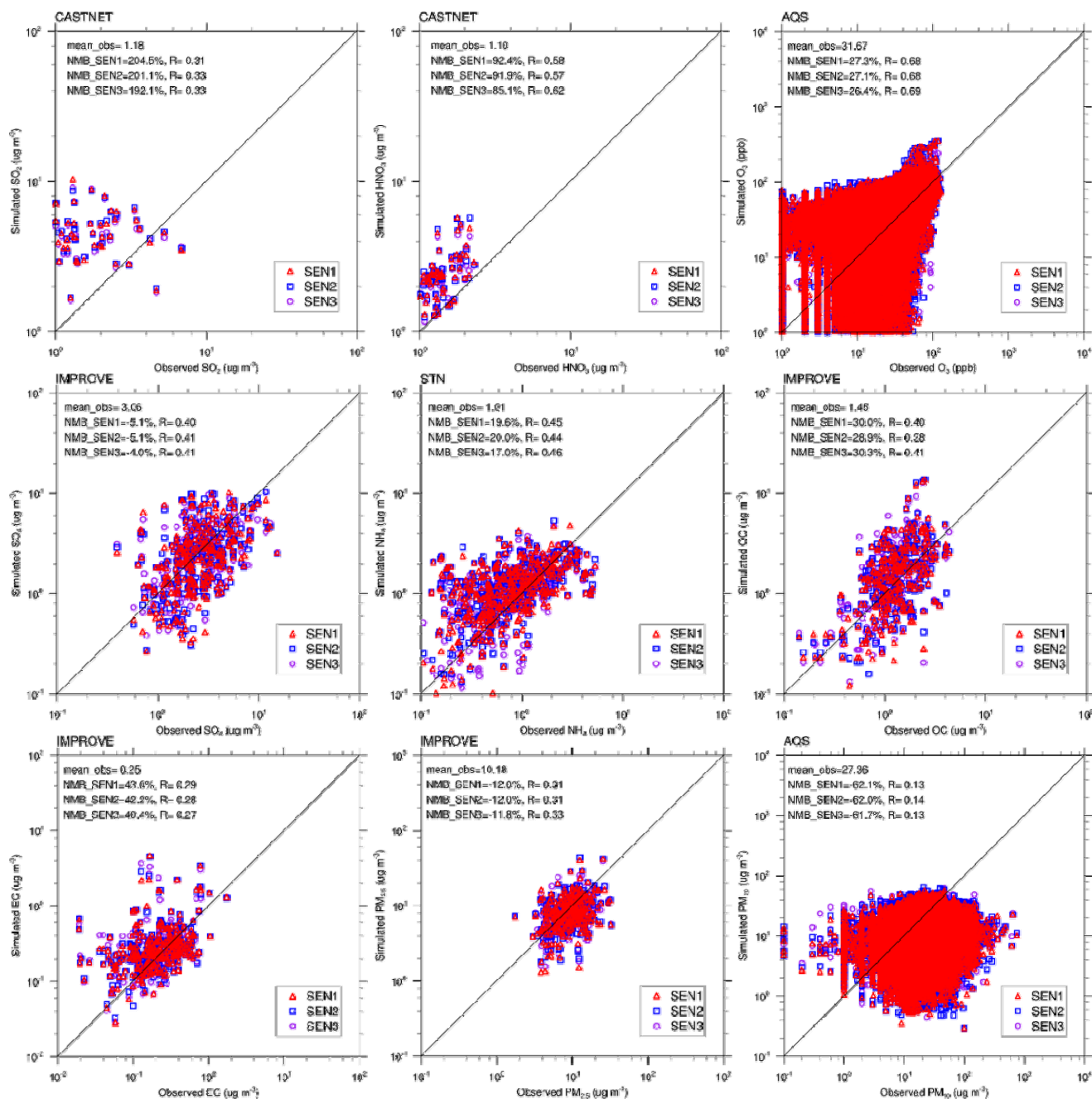
Fig. 10. Scatter plots of simulated vs. observed concentrations of major chemical species over different networks. SEN1: WRF/Chem standalone without coupling ocean model; SEN2: WRF/Chem coupling with 1-D ocean mixed layer model; SEN3: WRF/Chem coupling with 3-D ROMS.

and SEN3 overpredict AOD over land by 1.5% and 3.5%, respectively, and underpredict AOD over ocean by 34.6% and 31.5%, respectively. The underpredictions of AOD over ocean are likely due to the inaccurate predictions of marine aerosols (e.g., sea-salt) and overpredictions of precipitation over ocean. A detailed model evaluation could be found in Table S1(b).

Although the magnitudes of total column concentrations are not affected much by SEN3 compared to SEN1, the spatial distributions of some column species predicted by SEN3 can be affected through changes in large-scale

circulation, temperature, radiation, as well as precipitation through the coupling of WRF/Chem with 3-D ROMS. Fig. 12 shows the percentage differences for monthly-averaged column species between SEN3 and SEN1. Unlike the differences for column CO and O_3, which are within ± 5%, there are much larger differences in the spatial distributions for column NO_2, SO_2, and $PM_{2.5}$. For example, changes in column NO_2, SO_2, and $PM_{2.5}$ can be as large as 16.7%, 41.1%, and 31.1%, respectively. NO_2 and SO_2 can be oxidized to form HNO_3 and H_2SO_4, respectively, which can further produce secondary NO_3^- and SO_4^{2-} through
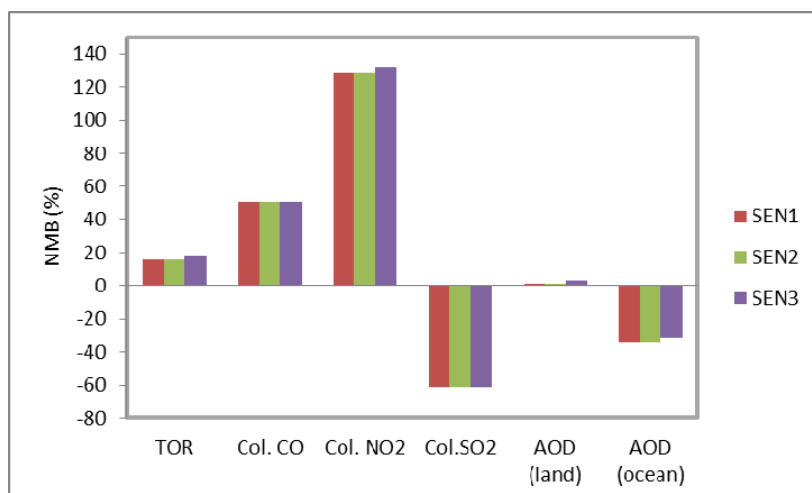
Fig. 11. The normalized mean bias (NMB, %) of column abundances of chemical species over the whole domain and AOD over land (left column) and ocean (right column) from SEN1 (WRF/Chem standalone, without coupling ocean model), SEN2 (WRF/Chem coupling with 1-D ocean mixing layer), and SEN3 (WRF/Chem coupling with 3-D ROMS).

gas-particle conversion, and thus affect PM concentrations. These processes involve chemical transformation, and aerosol dynamics and thermodynamics, which are affected by induced changes in meteorology through the coupling of 3-D ROMS. For example, significant increases for column abundances (e.g., NO_2, SO_2, and PM) over ocean are mainly due to the less wet scavenging through decreased precipitation over ocean as well as more stable boundary conditions predicted by SEN3. The decreases of SO_2 over land are likely due to more oxidation of SO_2 by OH radicals as well as increases of wet deposition through increases in precipitation over land. The changes in column NO_2 can also be attributed to changes in its reactions with volatile organic compounds through feedbacks on online biogenic emission calculations. The changes in column SO_2 and NO_2 could lead to changes in PM since they are gaseous precursors of NO_3^- and SO_4^{2-}. With the coupling of 3-D ROMS, the meteorological fields are affected, leading to changes in chemical transformations. These impacts are non-linear and complex, however, are non-negligible especially on regional scales.

CONCLUSIONS

In this work, 1-D OML and 3-D ROMS coupling with WRF/Chem are used to study the impacts of air-sea interactions on air quality predictions. With the inclusion of ocean coupling in SEN2 and SEN3, simulated boundary layer properties are changed. As OML is a simplified 1-D model with large uncertainty, the impacts on boundary layer are not as significant as those of the coupling of WRF/Chem with the 3-D ROMS, which consists of detailed primitive equations for 3-D ocean circulation and dynamics. Although SEN2 predicts SST, the coupling with the 1-D OML results in small changes in SST from the initial SST that is based on the NCEP reanalysis data. The warm bias of SST from SEN2 over Gulf Stream can generate larger monthly mean rainfall and surface latent

heat flux anomalies compared to SEN3. However, in SEN3, SST is prognostic and affected by additional processes (e.g., horizontal advection and Ekman transport processes), and therefore shows larger changes. Although additional possible tuning in the parameters in the 1D-OML model could lead to larger impacts on SST, the impact is less physically compared to that from the 3D-ROMS model. The lower precipitation in SEN3 than SEN1 is probably due to the changes in moisture flux convergence through large-scale changes in the circulation field and SST. The predictions of precipitation, LHFXL, and SHFLX are improved significantly in SEN3, with NMBs significantly reduced from 211.5% in SEN1 to 119.2% in SEN3, from 60.1% in SEN1 to 18.9% in SEN3, and from 138.2% in SEN1 to 50.2% in SEN3, respectively. However, compared to the observations of OAFlux, SST in SEN3 is slightly underpredicted with an NMB of –2.8%, which is mainly due to the lower initial conditions from global HYCOM data. Due to the improvement in the predictions of surface heat fluxes, PBLH predictions are also improved in SEN3, with NMBs reduced from 16.2% in SEN1 to –3.1% in SEN3 over ocean. Due to more stable boundary layer and less evaporation over ocean in SEN3, the predictions of most cloud variables such as CF, COT, and LWP over ocean are also improved in SEN3. As a result, the predictions of radiative variables such as SWD, OLR, SWCF, and LWCF over ocean are improved.

Due to the changes in the boundary layer properties, surface chemical predictions are affected significantly in SEN3. For example, With the coupling of WRF/Chem with 1-D OML model, surface levels of O_3 and $PM_{2.5}$ can increase as large as 1.8 ppb and 1.0 µg m^{-3}, and decreases as large as 1.4 ppb and 1.1 µg m^{-3}, with a domain averaged increase of 0.03 ppb and 0.02 µg m^{-3}, respectively. Through the coupling of WRF/Chem with the 3-D ROMS, surface O_3 and $PM_{2.5}$ concentrations can increase as large as 12.0 ppb and 3.0 µg m^{-3}, and decrease as large as 17.3 ppb and 7.9 µg m^{-3}, with a domain averaged decrease of 0.71 ppb
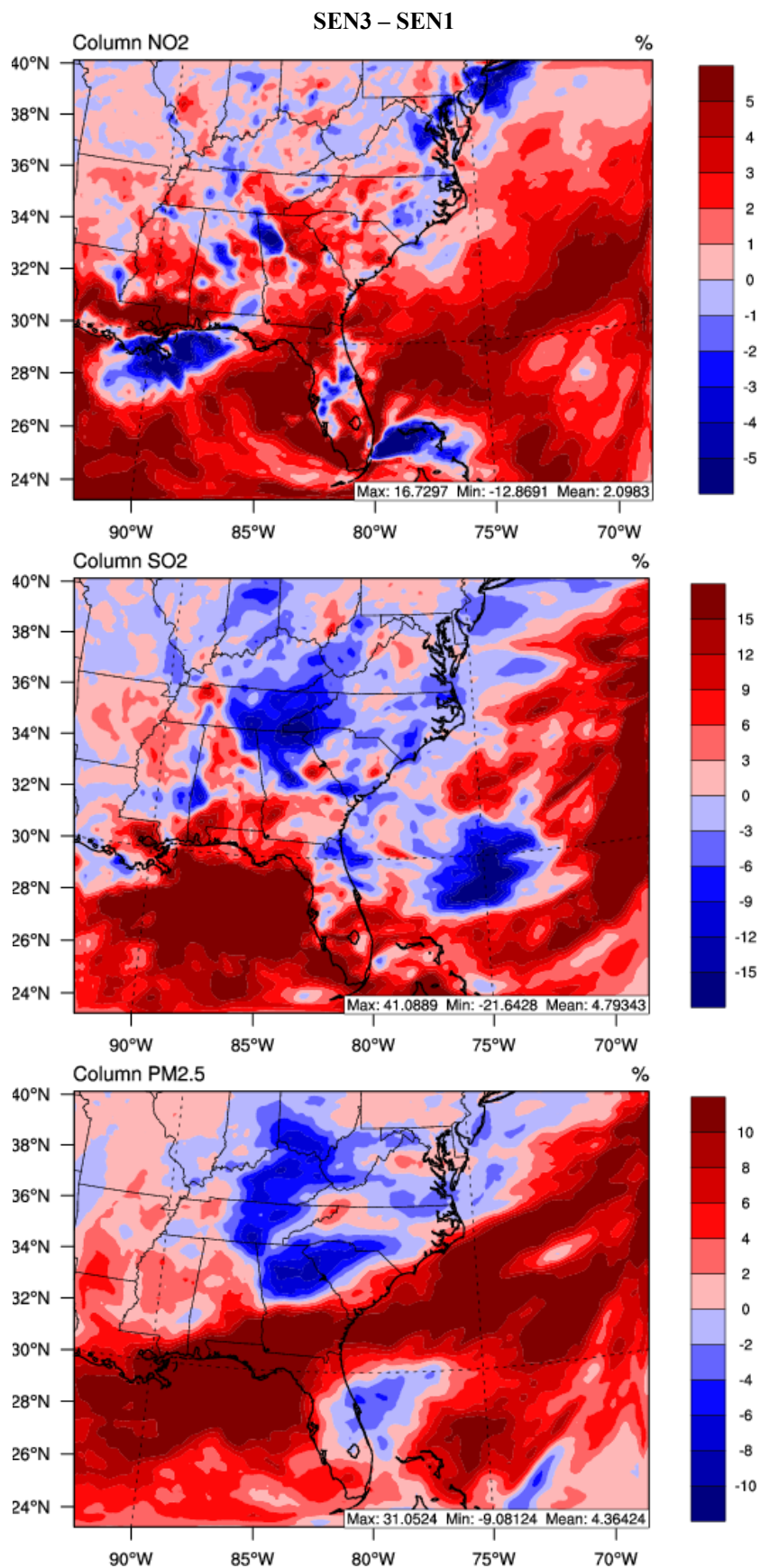
Fig. 12. The percentage differences of monthly-averaged column abundances between SEN3 (WRF/Chem coupling with 3-D ROMS) and SEN1 (WRF/Chem standalone without coupling ocean model).

and 0.08 µg m^{-3}, respectively. The largest differences in surface O_3 predictions are along the coastal areas and remote ocean, whereas the largest differences in surface $PM_{2.5}$ predictions are not only along the coastal areas and remote ocean, but also over inland areas, indicating the significant impacts of air-sea interactions on chemical predictions. Compared to SEN1, SEN3 shows overall better performance for chemical concentrations of SO_2, HNO_3, Max 1-h and 8-h O_3, SO_4^{2-}, NH_4^+, and NO_3^-, and PM_{10}. The simulated column concentrations are comparable in SEN1 and SEN3, with slightly better performance of column SO_2 in SEN3.

There are several limitations in this work. First, cold biases exist in the SST simulated by WRF/Chem-ROMS. Using an alternative ICs and BCs for ROMS based on other ocean models, such as the Global Ocean Physical Reanalysis System (GLORS) (http://www.cmcc.it/it/models /c-glors-the-cmcc-global-ocean-physical-reanalysis-system) and the Simple Ocean Data Assimilation (SODA) (http://www.atmos.umd.edu/~ocean/data.html) may reduce such cold biases in SST, which will in turn improve meteorological and chemical predictions of WRF/Chem-ROMS. Second, large biases remain in the predictions of some meteorological (e.g., WS10 over land and precipitation over ocean) and cloud variables (e.g., COT, CDNC, LWP, and SWCF), indicating the uncertainties in the model representations of boundary layer, convection, cloud dynamics and thermodynamics, as well as aerosol-cloud interactions. Those are the research areas that may lead to improved model performance for future work. Finally, when computational resources become available, finer grid resolution (e.g., 1–4 km) may be applied in the future to better capture the fine-scale features along the coast.

ACKNOWLEDGMENTS

SUPPLEMENTARY MATERIAL

Supplementary data associated with this article can be found in the online version at http://www.aaqr.org.

REFERENCES

Ahmadov, R., McKeen, S.A., Robinson, A.L., Bahreini, R., Middlebrook, A.M., de Gouw, J.A., Meagher, J., Hsie, E.Y., Edgerton, E., Shaw, S. and Trainer, M. (2012). A volatility basis set model for summertime secondary organic aerosols over the eastern United States in 2006. *J. Geophys. Res.* 117: D06301.

Alapaty, K., Herwehe, J.A., Otte, T.L., Nolte, C.G., Bullock, O.R., Mallard, M.S., Kain, J.S. and Dudhia, J. (2012). Introducing subgrid-scale cloud feedbacks to radiation for regional meteorological and climate modeling. *Geophys. Res. Lett.* 39: L24809.

Bennartz, R. (2007). Global assessment of marine boundary layer cloud droplet number concentration from satellite. *J. Geophys. Res.* 112: D02201.

Bernie, D., Woolnough, S., Slingo, J. and Guilyardi, E. (2005). Modeling diurnal and intraseasonal variability of the ocean mixed layer. *J. Clim.* 18: 1190–1202.

Binkowski, F.S. and Roselle, S.J. (2003). Models-3 Community multiscale air quality (CMAQ) model aerosol component, 1 Model description. *J. Geophys. Res.* 108: 4183.

Brayshaw, D. J., Hoskins, B. and Blackburn, M. (2011). The basic ingredients of the North Atlantic storm track, Part II: Sea surface temperatures. *J. Atmos. Sci.* 68: 1784–1805.

Byun, D.W. and Schere, K.L. (2006). Review of the governing equations, computational algorithms, and other components of the Models-3 Community Multiscale Air Quality (CMAQ) Modeling System. *Appl. Mech. Rev.* 59: 51–77.

Chelton, D.B., Schlax, M.G. and Samelson, R.M. (2007). Summertime coupling between sea surface temperature and wind stress in the Californi Current System. *J. Phys. Oceanogr.* 37: 495–517.

Chen, F., Miao, S., Tewari, M., Bao, J.W. and Kusaka, H. (2011). A numerical study of interactions between surface forcing and sea breeze circulations and their effects on stagnation in the greater Houston area. *J. Geophys. Res.* 116: D12105.

Eden, C., Greatbatch, R.J. and Boning, C.W. (2004). Adiabatically correcting an eddy-permitting model using large-scale hydrographic data: application to the Gulf Stream and the North Atlantic Current. *J. Phys. Oceanogr.* 34: 701–719.

ENVIRON (1998). User's Guide to the Comprehensive Air Quality Model with Extensions (CAMx) Version 2.0. http://www.camx.com, Last Access: June 2016.

ENVIRON (2010). User's guide to the Comprehensive Air Quality Model with Extensions (CAMx) Version 5.2. http://www.camx.com, Last Access: June 2016.

Fast, J.D., Gustafson, Jr., W.I., Easter, R.C., Zaveri, R.A., Barnard, J.C., Chapman, E.G. and Grell, G.A. (2006). Evolution of ozone, particulates, and aerosol direct forcing in an urban area using a new fully-coupled meteorology, chemistry, and aerosol model *J. Geophys.*

Res. 111: D21305.

Grell, G.A. and Freitas, S.R. (2014). A scale and aerosol aware stochastic convective parameterization for weather and air quality modeling. *Atmos. Chem. Phys.* 14: 5233–5250.

Grell, G.A., Peckham, S.E., Schmitz, R., McKeen, S.A., Frost, G., Skamarock, W.C. and Eder, B. (2005). Fully coupled "online" chemistry within the WRF model. *Atmos. Environ.* 39: 6957–6975.

He, J., Alapaty, K., Herwehe, J.A. and Bullock, Jr., R. (2017). Studying precipitation partitioning in multi-scale weather forecasts: Impacts of stability restoration methods. *Mon. Weather Rev., in Submitted*.

He, J., Zhang, Y., Glotfelty, T., He, R., Bennartz, R., Rausch, J. and Sartelet, K. (2015). Decadal simulation and comprehensive evaluation of CESM/CAM5.1 with advanced chemistry, aerosol microphysics, and aerosol-cloud interactions. *J. Adv. Model. Earth Syst.* 7: 110–141.

He, R. and Wilkin, J.L. (2006). Barotropic tides on the southeast New England shelf: A view from a hybrid data assimilative modeling approach. *J. Geophys. Res.* 111: C08002.

He, R., McGillicuddy, Jr., D.J., Keafer, B.A. and Anderson, D.M. (2008). Historic 2005 toxic bloom of Alexandrium fundyense in the western Gulf of Maine: 2. Coupled biological numerical modeling. *J. Geophys. Res.* 113: C07040.

Hofmeister, R., Burchard, H. and Beckers, J.M. (2010). Non-uniform adaptive vertical grids for 3D numerical ocean models. *Ocean Modell.* 33: 70–86.

Keeley, S.P.E., Sutton, R.T. and Shaffrey, L.C. (2012). The impact of North Atlantic sea surface temperature errors on the simulation of North Atlantic European region climate. *Q. J. R. Meteorol. Soc.* 138: 1774–1783.

Kushnir, Y. and Held, I.M. (1996). Equilibrium atmospheric response to North Atlantic SST anomalies. *J. Clim.* 9: 1208–1220.

Marchesiello, P., McWilliams, J.C. and Shchepetkin, A. (2003). Equilibrium structure and dynamics of the California current system. *J. Phys. Oceanogr.* 33: 753–783.

Nelson, J. and He, R. (2012). Effect of the Gulf Stream on winter extratropical cyclone outbreaks. *Atmos. Sci. Lett.* 13: 311–316.

Nelson, J., He, R., Warner, J.C. and Bane, J. (2014). Air–sea interactions during strong winter extratropical storms. *Ocean Dyn.* 64: 1233–1246.

Pollard, R.T., Rhines, P.B. and Thompson, R.O.R.Y. (1973). The deepening of the wind mixed layer. *Geophys. Fluid Dyn.* 3: 381–404.

Sarwar, G., Fahey, K., Napelenok, S., Roselle, S. and Mathur, R. (2011). Examining the impact of CMAQ model updates on aerosol sulfate predictions. The 10th Annual CMAS Models-3 User's Conference, October, Chapel Hill, NC.

Sarwar, G., Luecken, D., Yarwood, G., Whitten, G.Z. and Carter, W.P.L. (2008). Impact of an updated carbon bond mechanism on predictions from the CMAQ modeling system: Preliminary assessment. *J. Appl. Meteor. Clim.*

47: 3–14.

Seo, H., Subramanian, A.C., Miller, A.J. and Cavanaugh, N.R. (2014). Coupled impacts of the diurnal cycle of sea surface temperature on the Madden-Julian Oscillation. *J. Clim.* 27: 8422–8443.

Shapiro, G., Luneva, M., Pickering, J. and Storkey, D. (2013). The effect of various vertical discretization schemes and horizontal diffusion parameterization on the performance of a 3-D ocean model: The Black Sea case study. *Ocean Sci.* 9: 377–390.

Shchepetkin, A.F. and McWilliams, J.C. (2005). The Regional Ocean Modeling System: A split-explicit, free-surface, topography following coordinates ocean model. *Ocean Modell.* 9: 347–404.

Skamarock, W.C., Klemp, J.B., Dudhia, J., Gill, D.O., Barker, D.M., Duda, M.G., Huang, X.Y., Wang, W. and Powers, J.G. (2008). A description of the advanced research WRF Version 3. *NCAR Tech. Note NCAR/TN-475+STR*, 113 pp.

Thompson, G., Tewari, M., Ikeda, K., Tessendorf, S., Weeks, C., Otkin, J. and Kong, F. (2016). Explicitly-coupled cloud physics and radiation parameterizations and subsequent evaluation in WRF high-resolution convective forecasts. *Atmos. Res.* 168: 92–104.

Wang, K., Yahya, K., Zhang, Y., Wu, S.Y. and Grell, G. (2015a). Implementation and initial application of new chemistry-aerosol options in WRF/Chem for simulating secondary organic aerosols and aerosol indirect effects for regional air quality. *Atmos. Environ.* 115: 716–732.

Wang, K., Yahya, K., Zhang, Y., Christian, H., George, P., Christoph, K., Alma, H., Roberto, S.J., Juan, L.P., Pedro, J.G., Rocio, B., Paul, M. and Ralf, B. (2015b). A multi-model assessment for the 2006 and 2010 simulations under the Air Quality Model Evaluation International Initiative (AQMEII) phase 2 over North America: part II. Evaluation of column variable predictions using satellite data. *Atmos. Environ.* 115: 587–603.

Warner, J.C., Armstrong, B., He, R. and Zambon, J.B. (2010). Development of a coupled ocean-atmosphere-wave-sediment transport (COWAST) modeling system. *Ocean Modell.* 35: 230–244.

Willebrand, J., Barnier, B., Boening, C., Dieterich, C., Killworth, P.D., Le Provost, C., Jia, Y., Molines, J.M. and New, A.L. (2001). Circulation characteristics in three eddy-permitting models of the North Atlantic. *Prog. Oceanogr.* 48: 123–161.

Wu, R. and Kirtman, B.P. (2005). Roles of Indian and Pacific Ocean air-sea coupling in tropical atmospheric variability. *Clim. Dyn.* 25: 155–170.

Wu, R. and Kirtman, B.P. (2007). Regimes of seasonal air-sea interaction and implications for performance of forced simulations. *Clim. Dyn.* 29: 393–410.

Yahya, K., Wang, K., Gudoshava, M., Glotfelty, T. and Zhang, Y. (2014). Application of WRF/Chem over North America under the AQMEII Phase 2: Part I. Comprehensive evaluation of 2006 simulation. *Atmos. Environ.* 115: 733–755.

Yahya, K., Wang, K., Zhang, Y., Hogrefe, C., Pouliot, G. and Kleindienst, T. (2015). Application of WRF/Chem

version 3.4.1 over North America under the AQMEII Phase 2: Evaluation of 2010 application and responses of air quality and meteorology-chemistry interactions to changes in emissions and meteorology from 2006 to 2010. *Geosci. Model Dev.* 8: 2095–2117.

Yu, S., Mathur, R., Pleim, J., Wong, D., Gilliam, R., Alapaty, K., Zhao, C. and Liu, X. (2014). Aerosol indirect effect on the grid-scale clouds in the two-way coupled WRF-CMAQ: Model description, development, evaluation and regional analysis. *Atmos. Chem. Phys.* 14: 11247–11285.

Yu, S.C., Eder, B., Dennis, R., Chu, S.H. and Schwartz, S (2006). New unbiased symmetric metrics for evaluation of air quality models. *Atmos. Sci. Lett.* 7: 26–34.

Zambon, J.B., He, R. and Warner, J.C. (2014a). Investigation of Hurricane Ivan using the Coupled Ocean-Atmosphere-Wave-Sediment Transport (COAWST) Model. *Ocean Dyn.* 64: 1535–1554.

Zambon, J.B., He, R. and Warner, J.C. (2014b). Tropical to extratropical: Marine environmental changes associated with Superstorm Sandy prior to its landfall. *Geophys. Res. Lett.* 41: 8935–8943.

Zhang, Y., Liu, P., Pun, B. and Seigneur, C. (2006). A comprehensive performance evaluation of MM5-CMAQ for the Summer 1999 Southern Oxidants Study episode—Part I: Evaluation protocols, databases, and meteorological predictions. *Atmos. Environ.* 40: 4825–4838.

Zhang, Y., Vijayaraghavan, K., Wen, X.Y., Snell, H.E. and Jacobson, M.Z. (2009). Probing into regional ozone and particulate matter pollution in the United States: 1. A 1 year CMAQ simulation and evaluation using surface and satellite data. *J. Geophys. Res.* 114: D22304.

Zhang, Y., Pan, Y., Wang, K., Fast, J.D. and Grell, G.A. (2010). WRF/Chem-MADRID: Incorporation of an aerosol module into WRF/Chem and its initial application to the TexAQS2000 episode. *J. Geophys. Res.* 115: D18202.